THE ON-WATER INSTRUMENTATION OF A SPRINT CANOE PADDLE

THE ON-WATER INSTRUMENTATION OF A SPRINT CANOE PADDLE

BY

CAMERON GALIPEAU, B. ENG.

A Thesis
Submitted to the Department of Mechanical Engineering
and the School of Graduate Studies
of McMaster University
in Partial Fulfillment of the Requirements for the Degree of
Master of Applied Science

McMaster University MASTER OF APPLIED SCIENCE (2018)
Hamilton, Ontario (Mechanical Engineering)
TITLE: The On-water Instrumentation of a Sprint Canoe Paddle
AUTHOR: Cameron Galipeau
B.Eng.Mgmt, Mechanical Engineering and Management
McMaster University, Hamilton, Canada
SUPERVISOR: Dr. Stephen Tullis
NUMBER OF PAGES: xvi, 82

Lay Abstract

A measurement system for a sprint canoe paddle was created that can evaluate an athlete's stroke performance during race-like conditions. This system was tested using national-level athletes in a true on-water setting. By measuring the force and orientation of the athlete's strokes, the system was able to clearly distinguish the performance of various stroke techniques. Analysis of the force profiles and the derivation of stroke efficiencies provided additional performance indicators. This is the first system to achieve this amount of measurement detail of any rowing or paddling sport. This fully instrumented paddle system is ready to be used as a coaching tool to improve athlete performance. It can also be used as an academic tool for paddle blade study.

Abstract

A fully instrumented on-water sprint canoe system was designed, built, and tested. The system consists of: one 6-axis load cell in the paddle shaft at the blade, one inertial measuring unit (IMU) on the paddle, one IMU on the boat, and one GPS unit on the canoe boat. These sensors communicated wirelessly to a laptop where the data was processed and displayed in real-time. The sensors were rigorously tested and well-measured in their satisfactory accuracy. The system can provide a full decomposition of the blade water force into propulsive (forward/aft), side, and vertical forces. Previous systems for canoe have been extremely simple and rudimentary. There has been more effort in the rowing and kayak systems but they still failed to capture a full force profile.

On-water tests with national-level athletes examined a wide variety of sprint canoe strokes at different paces, power inputs, rates, and stroke lengths. The measurement system could clearly see the differences in force profiles between the stroke sets. A number of efficiency measures were developed using the available data. Instantaneous and integral in-stroke force ratios were developed based on the blade's propulsive force to total force proportion. Derived stroke averaged efficiencies also provided more information. These produced measurements of energy/impulse input to the boat's propulsion output. Differences in such efficiencies could be clearly seen in the various collected stroke sets.

This system will be highly useful to high performance athletes and coaches for modifying athlete technique. It has potential for improving equipment design and matching athletes to optimal blade styles. More academically, it can assist biomechanical assessments of sprint canoe and numerical flow studies around blades.

Acknowledgements

I would like to thank my supervisor, Dr. Stephen Tullis, for always providing clear and direct guidance. His advice to prioritize and focus on the important aspects lead me to the completion of this project.

Thank you to the athlete subject and lab-mate Dana Morgoch, who provided his talent and support for this thesis, and also the athlete Evan Bezemer, this thesis could not have been done without them. The Mississauga Canoe Club has produced excellent talent through their years, and I am thankful of their gracious facility use.

I need to thank the Mechanical Engineering Machine Shop team who provided the much needed practical advice of working a problem. I am grateful to have known Dan Wright, whose friendliness and knowledge will continue to inspire.

And, of course, a great thanks to my parents, siblings, and friends, who all have provided the support that goes beyond describable value.

Contents

List of Figures

List of Tables

List of Abbreviations and Symbols

α	Angle of oar force to boat direction (°)
β	Blade-in-water ratio
ϵ	Efficiency
η	Propulsion ratio
∇	Displacement m^3
ω	Pitch angular velocity of paddle (°)
ϕ	Roll angle of paddle (°)
ψ	Yaw angle of paddle (°)
θ	Pitch angle of paddle (°)
A	Acceleration vector (g)
a	Acceleration (g)
B	Boat beam (m)
C	Drag constant
C_B	Block coefficient
C_D	Drag coefficient
C_F	Friction drag coefficient
C_L	Lift coefficient
C_R	Residual drag coefficient
C_T	Total drag coefficient
D_b	Boat dissipation (W)
d_b	Forward boat distance (m)
D_O	Oar dissipation (W)
e_b	Blade efficiency
e_s	Shell efficiency
E_{Drag}	Dissipated drag energy (J)
E_{in}	Energy into water (J)

F_B Blade force (N)

F_D Drag force (N)

F_D Wet surface area (m^2)

F_P Propulsive force (N)

F_{Beq} Equivalent force (N)

F_{BP} Propulsive blade force (N)

F_f Fictitious force (N)

F_I Inertial vector forces (N)

F_S Side force (N)

F_V Vertical force (N)

F_{xyz} Respective load cell force reading (N)

Fr Froude number

J_B Blade impulse (Ns)

k Drag velocity coefficient

L Paddle length (m)

l Boat length (m)

L_B Paddle length from handle to CoP (m)

L_C Paddle length from handle to load cell (m)

L_H Paddle length from handle to bottom hand (m)

L_{Beq} Equivalent force location (m)

L_f Fictitious force location (m)

M_f Fictitious moment (Nm)

P Paddle power (W)

P_h Athlete handle power (W)

P_P Propulsive paddle power (W)

P_{wb} Propulsive power into water (W) (Kleshnev)

P_{ws} Lost shell power into water (W) (Kleshnev)

Re Reynolds number

T Boat draft (m)

t_{F_B}peak Time to peak blade force (s)

T_{xyz} Respective load cell torque reading (Nm)

V Boat velocity (m/s)

v_{BP} Aft/propulsive blade velocity (m/s)

v_B Blade velocity (m/s)

CFD Computational fluid dynamics

CoP Centre of pressure

DOF Degrees of freedom

IMU Inertial measuring unit

RMSD Root mean square deviation

spm strokes per minute

Chapter 1

Introduction

Sprint canoe, also called Canadian canoe or flatwater racing, is an internationally recognized Olympic sport that has a particular popularity in Canada. Sprint refers to the short distance racing, meaning the athletes work quickly to cross the finish line. In these races every millisecond counts. For example, the men's single 200 m finals in the 2016 Rio Olympic Games had a 0.538 s difference between 1st and 5th place [30].

In this thesis, the sprint canoe sport and its related research will be introduced and discussed (Chapter 1 & 2). It will show the necessity for a fully instrumented paddle and canoe (Chapter 2 & 3). The results will be displayed and an in-depth analysis of the measurements will follow (Chapter 4).

1.1 The Sport

There are a few variants in the sprint canoe sport used in the Olympics but the goal remains the same: to use a paddle to propel the canoe and cross the finish line before your competitors. The race categories are defined by the boat type (C: canoe, K: kayak), the number of athletes in the boat, and the race distance. For example, the canoe events for the 2020 Olympics will include men's C-1 and C-2 1000 m as well as women's C-1 200 m and C-2 1000 m. The International Canoe Federation (ICF) also governs and recognizes any combination of 1, 2, or 4 athletes with 100, 200, 1000, 5000 m race distances. The individual boat lanes are in a straight line except in some 5000 m races in which turns are allowed.

1.1.1 Rules

There are only a few rules for sprint canoe [28], some notable ones will help illustrate the sport. The athlete must keep the canoe paddle stroke to only one side of the canoe, to the preference of the athlete. The paddles must be single bladed and cannot be fixed to the boat in any manner. The canoe boats must adhere to some construction limitations such as: no steering rudder, hull geometries, maximum length, and minimum weight. In addition, materials and designs not reasonably accessible to all competitors are not allowed as they would provide an unfair advantage.

1.1.2 Equipment

The paddle consists of three parts: T-grip for the top hand, the shaft, and the blade. These parts are typically assembled with heat-glue, which allows for part specific customization. Wood was the most common material used until the mid-1980's when composites became the standard [9]. While more expensive, they are much lighter and stronger than wood. The blade shapes tend to be symmetrical and relatively flat with only a slight concave curve normal to the water force. The canoe boats are long and narrow with a relatively flat bottom hull. While they have limited drag, they are quite unstable and subject to capsizing for an inexperienced athlete.

1.2 Stroke Cycle

It is important to describe the stroke cycle and its phases as they will be referenced throughout this thesis. The phases, shown in Figure 1.1, are:

- **Setup:** athlete aligns paddle and body in an 'A' formation to prepare the blade's entry into the water.
- **Catch:** blade moves downward and enters water while rotating forward such that paddle becomes vertically aligned, the phase ends with blade fully immersed.
- **Drive:** also referred to as the draw or pulling phase, the submersed blade moves towards the aft of the boat.
- **Exit:** a sideways motion, called 'feathering' the blade, occurs to pull blade out of the water, the steering technique also occurs here.

- **Recovery:** blade is out of the water and athlete returns to the setup position.

(a) Setup **(b)** Catch **(c)** Drive/draw

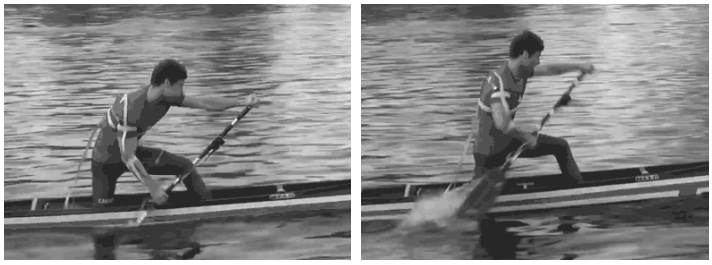

(d) Exit **(e)** Recovery

Figure 1.1: The five phases commonly used to describe one stroke cycle.

The phases are used to parse the stroke cycle for better analysis and coaching. The duration of each phase may vary across differing techniques which provides another analytical tool. The catch can be particularly important as it is easy to enter the water poorly, this can lead to air being dragged into the water behind the blade resulting in overall propulsive power loss [8].

The cycle itself is often used as a performance measure, such as number of strokes per minute and distance per stroke. There tends to be fewer strokes per minute (spm) for longer race distances; this fact must be considered when analyzing performance.

1.2.1 Blade Path

It is important to understand the path of the blade through the stroke as this governs the hydrodynamics surrounding the blade. With respect to the boat, it appears that the blade simply enters the water and drives backwards to provide propulsive force. Video motion capture by Morgoch and Tullis [44], seen in Figure 1.2, provided position data of the paddle and canoe throughout one stroke perpendicular to the canoe's direction of travel. Something to note - it appears that the top hand has only a small amount of horizontal motion up until the end of the drive phase.

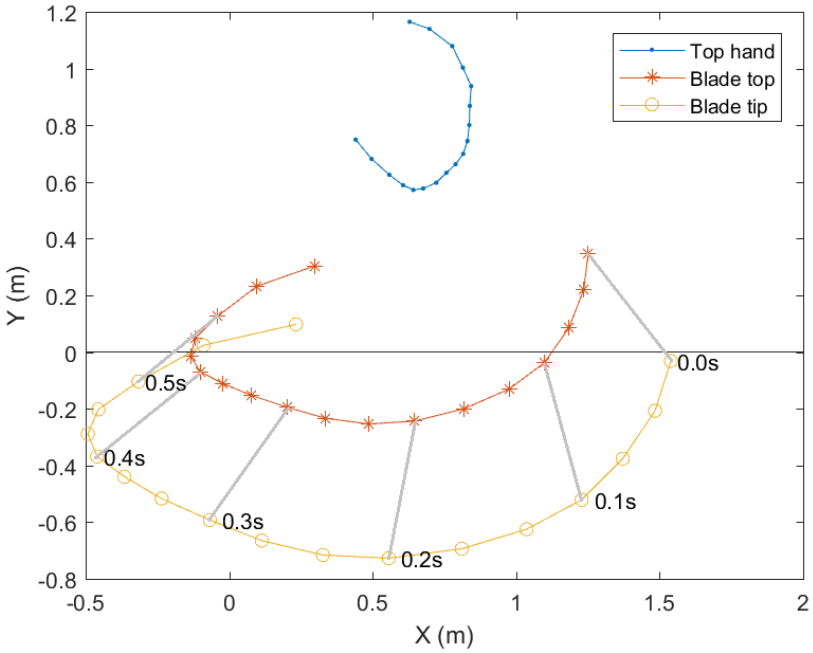

Figure 1.2: The path of the paddle and blade with respect to the boat, viewed laterally. The blade (shown as grey line) enters water on the right side of the figure at $t = 0.0\,\text{s}$, sweeps backwards towards the aft, then exits towards the left side of the figure. Data from Morgoch and Tullis [44].

The blade path with respect to the ground (i.e. stationary water) is quite different. Figure 1.3 shows how the water sees the blade as it enters and exits the water. There is a surprisingly small amount of horizontal motion; the tip of the blade enters at a steep vertical angle, makes a 'ribbon' shape, then leaves the water at a very shallow vertical angle. The top of the blade enters and exits the water all while travelling towards the bow of the boat. This leaves a portion of the top blade face to encounter adversely propulsive water flow. This blade path indicates that there are more complicated flows than a just a flat blade pushing water towards the aft to provide propulsion.

It is difficult to properly study the blade hydrodynamics, which will become apparent in the Literature Review chapter. The combination of different athletes, nonidentical strokes, equipment, environment, and available instruments result in systems that require simplifications. Some common assumptions, as it will be shown, are major aspects of the stroke. Whether it's a computational fluid dynamics (CFD) approach or an on-water data acquisition, there often are assumptions that result in the study having an incomplete story of the stroke. Without sufficient information, adverse

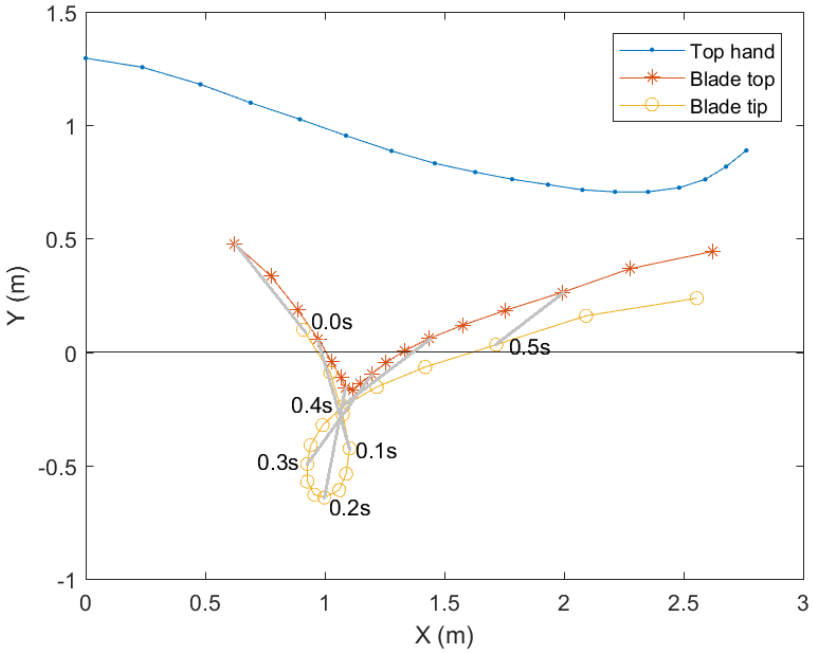

Figure 1.3: The path of the paddle and blade with respect to the ground looking laterally to the canoe's direction. Blade (shown as grey line) enters water on the left at $t = 0.0\,\mathrm{s}$ and exits towards the right side of the figure. Data from Morgoch and Tullis [44].

coaching or athletic decisions could be made.

Chapter 2

Literature Review

Performance improvements have been realized from years of tracking and analyzing aquatic sports. This improvement is thanks to greater aerobic capacity, better equipment, and better training [54]. Studies along the way helped understand and shape the future of the rowing, kayak, and canoe sports. The focus is often from a biomechanical, numerical, or experimental viewpoint and varies between athlete and equipment performance. A considerable amount of work has been done in the rowing and kayak fields, but there is a lack of study effort into the sprint canoe by the community. Parallels can be drawn from the different sports as they are not completely incompatible; care must be taken when making conclusions. There are also numerous biomechanical studies across many other sports that strictly analyze athletic performance. However, the scope of this thesis focuses on the potential of the instrumented system and various analyses using the acquired data.

2.1 Hydrodynamics

Experimental measurements of flow dynamics around a variety of blades types has been completed. Coefficients of drag and lift (C_D and C_L respectively) of various blades have been determined a number of times, usually by means of a quasi-static approach [43]. Caplan and Gardner [13] used this quasi-static approach to compare the popular Big Blade and Macon rowing blades. They used scaled models in a flume and measured normal and tangential oar forces using strain gauges at static angles to the free stream. The authors contested this quasi-static method is reasonable since true propulsive and quasi-static approaches differ to within 5% of each other when

comparing front crawl swimming [6]. However, the rowing blade path is different to a swimmer's hand and involves much higher forces, the unsteady results would likely differ due to residual and developing flows from the unsteady blade path. This was investigated by Sliasas and Tullis [55] using CFD by comparing a full sized model of the quasi-static state experiment in Caplan and Gardner [13] to an unsteady flow simulation. It was found that C_D and C_L values differed considerably between the quasi-static and unsteady flows due to the transient formation and shedding of vortices and free surface deformations. From this, it was concluded that the complex blade motions and flows cannot be determined by steady experiments alone.

The rowing and canoe blade paths have a number of similarities and differences. The oar blade's centre stroke path resembles a figure-9 shape in the horizontal plane [34] with the canoe's blade path having a similar shape but in the vertical plane. With similar blade shapes and angles of attack, it is expected that similar flow behaviour would occur. However, significant differences alter the outcomes, such as the canoe's shorter catch phase and the vortices formed from the blade shape and orientation [55, 44]. In addition, surface deformations from the rowing blade's top edge affects hydrodynamics differently than the top portion of the canoe blade.

As with all fluid topics, the recent availability of CFD resources has sparked a number of papers revolving around kayaking, rowing, and canoeing. Little work has been done in the canoeing sport, but recent numerical analysis found a significant drop in propulsive force due to back pressure at the top of the blade during the late catch phase of the stroke [44, 43]. A simple adjustment of technique or blade design could remedy this and increase total propulsive force. This potential benefit warrants further investigation.

All numerical results should be validated by measurement, there have been numerous attempts to accomplish this with varying degrees of success. While few have been for the canoe sport, technological advancements across all self-propelled aquatic sports should be considered. The similar conditions offer great starting blocks so some notable ones will be reviewed.

2.2 Instrumentation

There are numerous ways to measure performance or analyze biomechanical aspects of these water sports. On-water methods became possible by the technological ad-

vancements in the 1960s, allowing video capture, strain gauges, data logging, and FM telemetry. These methods offer data resembling true mechanics of the sport but are often difficult to implement. Off-water methods can be done in a controlled manner but often simplify the mechanics. Some methods include athletes on ergometers or flume testing of various equipment. The following sections will review various on-water methods.

2.2.1 Video Capture

An early use of video capture was completed in 1979 by Plagenhoef [50] by filming numerous Olympic canoe and kayak athletes over a nine year period. The author was able to notice differences based on a paddler's skill level as well as long-term trends of the same athlete. It was found that the stroke rate was the best indicator of determining performance. Plagenhoef also found that the best canoeists decreased trunk movement (body movement) at the catch phase, which decreased the vertical bobbing motion (heave) of the boat. Plangenhoef found that minimal top hand movement was a trait found among the best canoeists. The static top hand ensured a high paddle pivot point which flattened the blade arc for better propulsion.

In 1980 Martin and Bernfield [38] used video capture to examine the relationship of shell velocity, stroke phases, and stroke rate. The authors found that a significant positive relationship exists for stroke rate and average shell velocity. Also, a greater force during the drive and shorter recovery resulted in a faster rowing velocity. The amplitude of the shell velocity throughout the stroke and its relationship to average velocity and stroke rate was also investigated. The theory was that minimal velocity amplitude meant higher boat efficiency in terms of hull drag. However, no significant relationship was found.

These early studies proved the capability and potential of video data acquisition in the water sports. While the kinetic analysis lacked important data such as paddle force, many important parameters could still be analyzed which undoubtedly benefited the sport.

2.2.2 Instrumentation Devices Review

There have been a number of on-water instrumentation systems in rowing and kayak, but very limited in the canoe sport, as shown in the list of systems in Table 2.1. This

Year	Author(s)	Sport	Method
1971	Ishiko [31]	R	Strain gauges on shaft, accelerometer on boat, FM telemetry
1974	Vos et al. [65]	R,C	Strain gauges on shaft, FM telemetry
1974	Celentano et al. [17]	R	Strain gauges and orientation potentiometer on oar lock
1986	Stothart et al. [62]	K,C	Strain gauge on canoe shaft, FM data transmitter
1989	Smith and Spinks [58]	R	Strain gauged oar shaft, shaft orientation potentiometer, railing turbine for boat velocity, FM telemetry
1992	Aitken and Neal [1]	K	Multiple strain gauged shaft
1995	Peach et al. [48]	K,R,C	Video capture, accelerometer on boat
1999	Kleshnev [34]	R	Proximity sensor for bending shaft, oar orientation by potentiometer, accelerometer and electromagnetic sensor for boat velocity
2009	Ho et al. [27]	DB	Strain gauge on shaft and video capture
2010	Mattes and Schaffert [39]	R	Rowing shell GPS and accelerometer
2010	Schaffert et al. [53]	R	Rowing shell GPS and accelerometer with real-time audio feedback to athlete
2011	Helmer et al. [25]	K	Pressure sensors on blade, accelerometers on athlete
2011	Gomes et al. [22]	K	Multiple strain gauged shaft
2011	Tessendorf et al. [64]	R	One IMU on each oar and one IMU on rowing shell
2012	Fleming et al. [20]	K	Strain gauge on-water vs. strain gauge on-ergometer
2013	Sturm et al. [63]	K	Attached strain gauged cantilever nodes, inertial measuring units, wireless to Android
2016	Morgoch et al. [45]	C	Multiple strain gauged canoe shaft, inertial paddle orientation

Table 2.1: List of notable instrumented on-water systems. R: rowing, K: kayak, C: canoe, DB: dragon boat.

table includes all of the notable systems known at the time of writing. It is clear that the most systems use strain gauges to determine blade force by measuring the bending moment of the shaft. It is also evident that many systems include an accelerometer and/or GPS unit on the boat as well. A more detailed description of some of the notable systems follows.

An early canoe instrumentation attempt in 1986 by Stothart et al. [62] used full Wheatstone bridge strain gauges on wooden canoe paddles to collect data on bending force on the shaft of the paddle. The system had issues with heavy equipment required onboard the canoe, though it included an FM transmitter for data telemetry.

This proof-of-concept research provided no data however, it showed a possibility for a practical instrumentation system.

In 1993, Pelham et al. [49] found that using accelerometers in boats enabled the ability to quantify the performance of varying parameters. The team successfully analyzed video and logged accelerometer data to determine velocity outcomes between different subjects, technique, and equipment. A similar system was used by the same group Carter et al. [16] in 1994. It is now common practice for teams to place a GPS/accelerometer combination sensor on the canoe, allowing simple post-practice analysis of speed and discrete acceleration data. Athletes can try different techniques and observe the resulting speed and acceleration or track their performance throughout seasons.

In 1992 Aitken and Neal [1] used strain gauges on a kayak shaft and presented a force profile along with a number of parameters such as peak force, impulse, time to peak force, and blade-in-water time. The authors claimed their system provided athlete power, however, it was not presented and it is unknown how power was calculated.

A study that captured kayak paddle forces was completed by Gomes et al. [22]. The alignment of four quarter Wheatstone bridges placed along the paddle shaft provided two-plane force profiles of the two blades. These additional bridges set at 90° to the blade plane allowed for a more comprehensive kayak force profile. This enabled a comparison of left/right hand strokes and starting strokes to moving strokes using two-plane forces. Note that the assumption of centre of the blade is the centre of pressure was used, the implications of this assumption will be discussed later in this thesis.

More recently, Sturm et al. [63] used two strain gauged cantilevers attached to the kayak shaft at two different planes near each of the blades. In addition, inertial sensors (accelerometer and gyroscope) were placed on the paddle. The system was modular which allowed the athlete to use his own equipment. It proved to be a useful practical tool in obtaining force profiles of the paddle. However, the force on the kayak blade was assumed to be in the middle of the blade face. Also, due to technical restrictions, the placement of the sensor nodes caused errors in one of the planes of force measurement. The modular approach of this system is something to note, as the proper athlete equipment is an important factor in instrumentation.

A different approach to paddle instrumentation was done by Helmer et al. [25]. These researchers placed pressure sensors on the blade face and were able to determine

the depth of both blades throughout each stroke. Athlete elbow angles were also measured by attached accelerometers. However, force on the blade or any hydrodynamic interaction was not resolved.

The numerous systems range in their use from a practical performance tool to a strictly academic study. As time progresses and technology advances, more variables are being considered. In recent years, the trend is towards multi-device instrumentation. The small modern devices allow inertial and strain sensors to be used in one system. The early systems suffered from large heavy equipment and technical difficulties of transmitting and storing data [62].

A promising instrumented kayak system dubbed the 'E-kayak' produced by Bifaretti et al. [7] will provide multiple parameters in real time. Their system includes a GPS, a 6 degrees of freedom (DOF) inertial measuring unit (IMU), a foot-brace force sensor, and a paddle force sensor. These are all streamed to an Android smartphone or tablet. The 6-DOF IMU includes a linear accelerometer and gyroscope, each measuring three axes. The system is in the prototype development stage however, the focus on full instrumentation with user-friendly practicality is something to note.

As of writing, no other research has been successful in obtaining the true blade force and its location on the blade. Previous work by the author used series of strain gauges along the paddle shaft attempted to resolve the centre of pressure (CoP), however, this was not sufficiently accurate [45]. The principle for determining force from the strain gauges was fairly simple. Four sets of full Wheatstone bridges in bending were used to interpolate and extrapolate the resulting moment diagram. If the gauges could provide the complete moment diagram, the location of the force could also be determined. The problem was that the two sets of gauges in-between the blade and the bottom hand had to be very close together due to spacing of the hand and the blade stem. This accuracy of the CoP using the Wheatstone bridges was found to be $\pm 6\,\text{cm}$ using three-point bench load testing of weights up to $30\,\text{kg}$. This provided little reliable information of the CoP movement on a blade that is only $50\,\text{cm}$ long.

A lack of on-water experimental canoe work is quite evident, as most examples shown above are for kayak and rowing. No known experimental study has accurately been able to find the location of blade force (i.e. centre of pressure). It appears that all cases assumed the force acted in the middle of the blade. This leaves question to the accuracy of a resolved blade force and how the force develops on the blade throughout the stroke.

2.3 Performance Indicators

The objective from a coaching point of view is to analyze the performance parameters of the athlete and determine what is needed to improve athletic outcome. Tracking boat velocity and using ergometers are excellent performance measures, however, to take it to the next level of analysis, more information is needed. This gets difficult very quickly with added complexity such as the canoe's blade path. Some common [3] performance indicators include:

- peak force
- power
- impulse
- stroke rate
- stroke length
- stroke distance
- blade submerged ratio
- boat speed variation

A number of misconceptions can arise and lead to misinformed decisions. It is important that terminology and the presentation of data is clear and justified. Some indicators, such as efficiency and blade slip, are typically only found in literature, all of which will be investigated in this thesis.

2.3.1 Efficiency

Getting every percentage point of efficiency is often the most importance factor in engineering. This is also true for all racing sports where getting more out of the same input work is paramount. However, a proper measure of efficiency is a practical problem in canoeing. Perfect efficiency implies that the work done by the athlete is pure momentum transfer into the boat. From this, it would seem that all interactions with the water is some sort of resistance and detrimental to total efficiency. It was believed by some analysts that the blade slipping through the water was a source of inefficiency [23, 52]. However, that is believed to be a misconception [14] as the slip of the blade through the water can produce positive propulsive forces [46].

Sometimes the term *efficiency* refers to the propulsive to blade force ratio. Intuitively speaking, one would want to maximize propulsive forces to increase forward motion, while minimizing vertical and side forces which do not directly contribute to forward velocity. This ratio η, simply tells how much propulsive force F_P is achieved

from the total blade force F_T, which is

$$\eta = \frac{F_P}{F_T} \tag{2.1}$$

A similar approach using power instead of force was described by Kleshnev [34]. This approach has an advantage as this can provide an instantaneous measure as to how the paddle is oriented through its stroke. An extended version of this approach was used for determining dragon boat efficiency on a per-stroke basis by Ho et al. [27]. The approach was

$$\text{Paddling efficiency} = \frac{\text{propulsive blade energy}}{\text{total blade produced energy}} \tag{2.2}$$

which is equivalent to

$$\eta_{Ho} = \frac{\int F_{Bp} v_{Bp} dt}{\int F_B v_B dt} \tag{2.3}$$

of each stroke. Here, the blade force and blade velocity (F_B and v_B), and their respective propulsive components (F_{Bp} and v_{Bp}), are used in an integrated ratio across the stroke.

While maximizing the propulsive force ratio is encouraged, it may be impossible to do as some vertical component is required to support the canoeist during the catch [8]. Conversely, previous measurements found relatively little vertical force during the catch [44]. This suggests there is only a small amount of potential propulsive improvements during the catch and early drive phase.

Efficiency has been calculated by numerous methods through various definitions as reviewed by Cabrera and Ruina [10]. There are many athlete and equipment motions occurring that make this a difficult measure. Throughout a stroke, the boat is pitching, rolling, heaving, surging. To a lesser extent, the boat is also yawing and swaying. In addition, the paddle is entering, drawing, and recovering out of the water in complex motion. Power into the system, provided by the athlete, and out of the system, dissipated through drag, is not a simple measurement and will require assumptions and analysis. A few simplifications can make this concept more measurable, such as to neglect all motions of the canoe to except for 1D forward motion. Another is to simplify athletic motion, where only work into the water is accounted for.

Cabrera and Ruina [10] used work to define rowing efficiency as

$$\epsilon = \frac{D_b}{D_b + D_O} \tag{2.4}$$

where D_b is boat dissipation and D_O is the oar dissipation. This was calculated using their on-water data, the terms were defined as

$$D_b = C \int V^3 dt \tag{2.5}$$

$$D_O = \int F_{oar} v_{Bp} dt \tag{2.6}$$

where C is a combined drag constant, V is the boat velocity, and v_{Bp} is the relative propulsive blade velocity. The v_{Bp} term is essentially slip velocity; the authors explain that oar efficiency is maximized by minimizing slip and that a very large blade would suffice to having near-perfect efficiency. A large blade would be at the cost of other factors such as weight, which may offset its benefits.

Kleshnev [34] had a different definition of efficiency by separating blade efficiency e_b and shell (boat) efficiency e_s. Blade efficiency was defined as

$$e_b = \frac{P_h - P_{wb}}{P_h} \tag{2.7}$$

where P_h is the power input at the handle and P_{wb} is the propulsive waste power at the water, computed by

$$P_{wb} = F_B v_s \cos(\alpha)$$

where F_B and v_s are the force and slip velocity of the blade respectively. Angle α is the angle between the force and water velocity flow against the blade. Similarly, e_s is calculated using

$$e_s = \frac{P_p - P_{ws}}{P_p} \tag{2.8}$$

where P_p is the instantaneous propulsive power (same as $P_h - P_{wb}$) and P_{ws} is the shell power lost due to velocity fluctuations given by

$$P_{ws} = C_D V_i^3 - C_D \overline{V}^3 \tag{2.9}$$

where C_D is a drag coefficient constant, V_i is the instantaneous velocity, and $\overline{V}$ is the

average velocity over the stroke cycle. The product of e_b and e_s gives total mechanical efficiency e. The author also defined a *propulsive effectiveness* f by adding a factor V_i/V_{max} to the efficiency definition that allowed the instantaneous boat velocity versus a maximum velocity. This was done so that a fast, moderately efficient stroke can yield a higher effectiveness than a slow, efficient stroke. By separating the shell and blade efficiencies, Kleshnev found that improving of blade efficiency yielded greater rowing performance than improving shell efficiency.

These presented efficiency estimations are only a few examples. While a theoretical efficiency can be discussed, it is difficult to measure given available technology and practicality. These methods attempt to provide a reasonable efficiency calculation with their instrumentation systems. Regardless of the method, it is clear that a few aspects must be measured: paddle force, velocity, and orientation. Of course these must be measured against the outcome—the canoe's velocity.

2.3.2 Physiological Efficiency

So far, the mechanical efficiency of paddling and rowing has been discussed. However, the physiological efficiency is considerably important and should not be neglected. While physiological efficiency is not measured in this thesis, this review will shed light on the important factors that the instrumented paddle could analyze in the future.

Every individual has a unique physiology, meaning a certain cycle cadence and paddle force produces the optimum output [61]. This is in part due to the force-velocity relationship, where a muscle's velocity of shortening decreases as isotonic muscle load increases. This widely used [33] relationship was described by Hill [26] using

$$(F + a)v = b(F_0 - L) \tag{2.10}$$

where a and b are coefficients, and with F and F_0 being the applied load and isometric load respectively. Applying this to a rowing ergometer [24, 60], a multi-athlete force-velocity relationship along with the measured power curve was produced, shown in Figure 2.1. From this, it is apparent that an athlete has a peak power output at a specific force and velocity.

High efficiency is achieved if the athlete operates in his/her optimal power output range for the longest possible duration. With this, a physiological efficiency is proposed

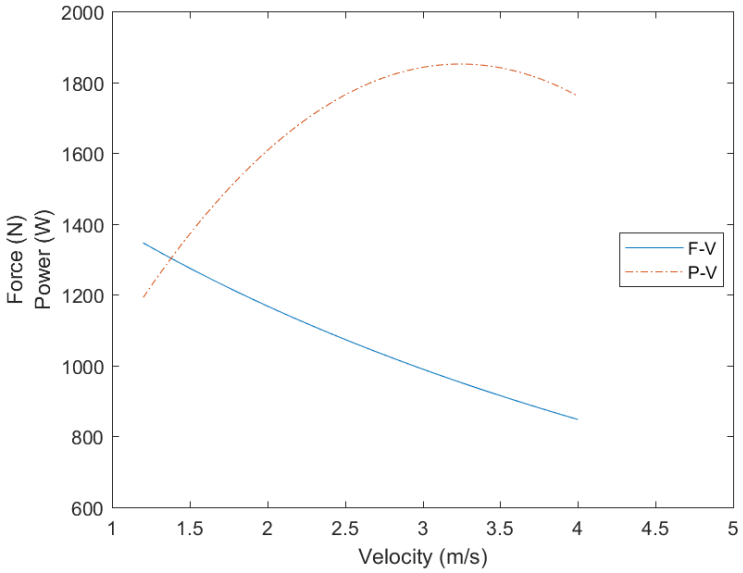

Figure 2.1: The force-velocity (F-V) and power-velocity (P-V) relationship of a rower, data from Sprague IV et al. [60]

as

$$\epsilon_{physio} = \frac{\text{measured average power}}{\text{known power capability}} \tag{2.11}$$

where the measured power is that of the athlete, given by the product of the instantaneous force and velocity of the athlete's bottom power hand.

Matching the athlete's on-water results to known optimal force-velocity relationship can offer a significant advantage. A blade size adjustment has been found to be able to increase performance by use of matching force-velocity profiles [61]. Another possibility is to simply adjust the shaft length or hand positions to change the applied torque. There are also aerobic and anaerobic training considerations that could be improved by using appropriate on-water data.

2.4 Objectives

There is a clear lack of on-water experiments in the sprint canoe sport; a fully instrumented system has not been built. Many rowing and kayak instrumentation systems exist, but they tend to oversimplify the mechanics and assume that shaft bending is an accurate portrayal of the blade forces. The goal of this thesis is to show that a complete blade force profile is critical to performance analysis. It will be shown

that merging data from multiple sensors provides additional worthy information. A first of its kind fully instrumented system was needed for the paddling sport, the following chapter will show how this was accomplished. A full demonstration of its measurement capability will be shown, specifically the performance parameters that enable a physical analysis of technique and stroke efficiency.

Chapter 3

Methodology

This chapter will describe the decision process of each selected device on the instrumentation system. The method of device implementation and the resulting capabilities will also be discussed.

3.1 Instruments

Before the instruments were selected, the variables to measure needed to be decided. Orientation of the boat and paddle, force on the blade, and speed of the boat were all required for this study to be useful. It was also imperative that the instrumentation system did not hinder athletic performance. The system needed to collect the data in real-time during race-like conditions.

As discussed in the previous chapter, it is clear that numerous data acquisition systems have existed. However, none have been capable of providing true blade force, centre of pressure, athlete power, or a full three-axis force profile. To accomplish this two inertial measuring units (IMUs), one load cell, and one GPS were incorporated into the athlete's paddle and canoe. The data streams were sent over wireless means to a laptop in the coach boat which was then processed and displayed in real-time using LabVIEW. The system's configuration is shown in Figure 3.1.

The two major elements that needed to be measured were force on the blade and the orientation of the paddle. Knowing the blade's orientation compared to the boat would enable the blade force F_B to be broken down to its propulsive F_P, and side F_S, and vertical F_V components. These components are equivalent to the boat's orientation of x_B, y_B, and z_B respectively, which is shown in Figure 3.2. The paddle

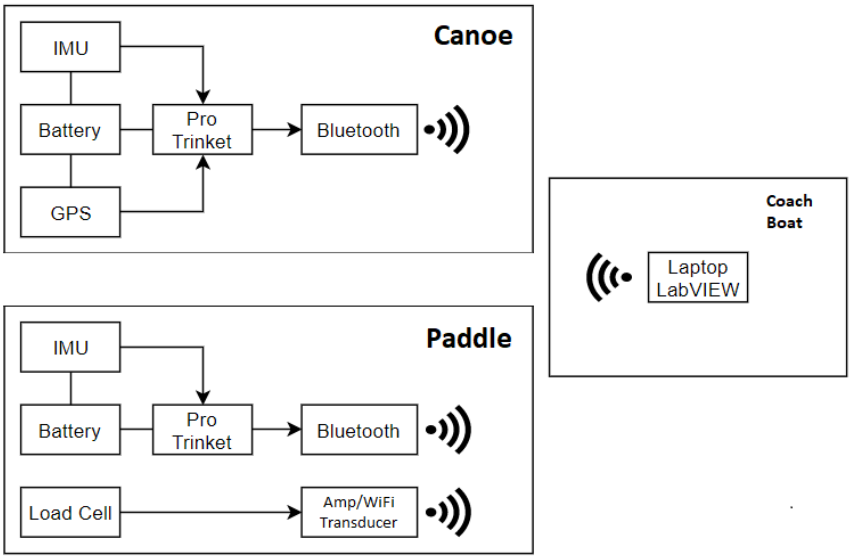

Figure 3.1: Block diagram of all the devices used in the instrumentation system. Arrow indicates data flow direction, laptop receives data over Bluetooth from the Pro Trinket (Arduino) connected devices, while the wireless transducer transmits over TCP/IP.

has its own coordinate system that is defined by the load cell that is fixed to the paddle's shaft (see Figure 3.2 and 3.5). The axis and orientation relationship can be seen in Figure 3.3.

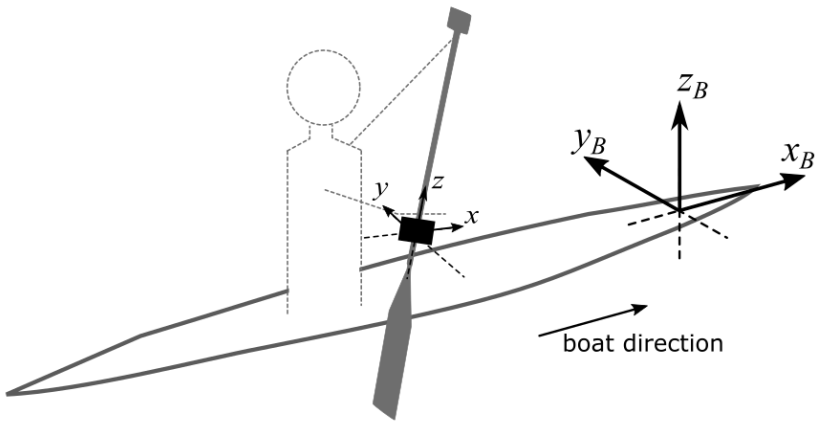

Figure 3.2: Axis definitions of the boat x_B, y_B and z_B where the canoe travels in the x_B direction. Paddle axis definitions x,y, and z shown at load cell.

The orientation angles of the paddle and boat similarly defined. To relate the orientation to Euler angles pitch θ, roll ϕ, and yaw ψ, the paddle is imagined to align its xyz axes with the boat's $x_B y_B z_B$ axes. This would make the paddle vertically

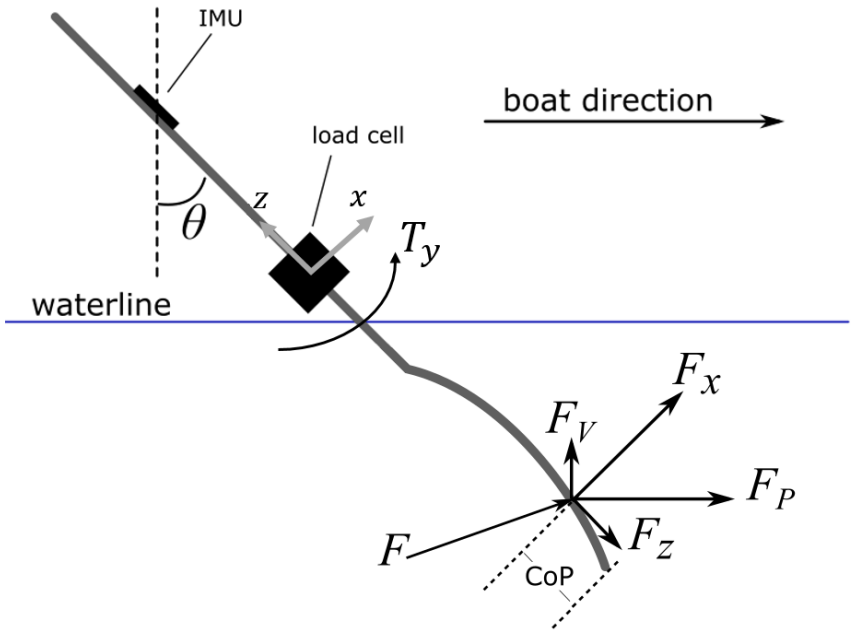

Figure 3.3: The paddle viewed from the side (boat's $x_B z_B$ plane). The load cell measures forces hypothetical force F as F_x, F_z, and T_y in its own coordinate system giving the CoP. These are rotated using the paddle orientation (pitch angle θ shown) into the propulsive F_P and vertical F_V forces. Direction y is into the page corresponds with side force F_S.

aligned (as it is in the late-catch phase). The orientation angles for the boat and paddle then work as:

- positive pitch θ: clockwise about y axis
- positive roll ϕ: clockwise about x axis
- positive yaw ψ: clockwise about z axis

3.1.1 Inertial Measuring Units

Modern inertial measuring units (IMU) are very small and typically use the I^2C protocol. This enables these inexpensive yet powerful devices to be implemented across many platforms making them useful in a wide range of applications. In this system, two LSM9DS0 Adafruit IMUs were used along with an Adafruit 5 V Pro Trinket Arduino based controller. These IMUs measure nine degrees of freedom (9-DOF), meaning it measures 3-axes each of linear acceleration, angular velocity, and magnetic flux density from the accelerometer, gyroscope, and magnetometer devices respectively.

The stream of data is timestamped and input to LabVIEW at 100 Hz where it is processed, displayed, and recorded. An open source algorithm [4] developed by Euston et al. [19] commonly used in drone technology was implemented in LabVIEW to resolve the raw data into orientation. This final data output is then a quaternion orientation aligned from up-down and north-wise directions. For viewing simplicity, the quaternions are transformed into Euler angles for display. The IMU was statically and dynamically tested to provide accurate orientation readings of $\pm 1.5°$. See details on these tests in Appendix B.

Bluetooth modules and batteries were added to allow wireless communication from the devices to the coach boat laptop. For each device on the paddle, small protective enclosures were created from 3 mm thick laser-cut acrylic then waterproofed with sealant wrapping. The IMU on the paddle was strapped and taped on the shaft in-between the athlete's hands. The IMU on the canoe was secured in an acrylic box along with the Arduino, GPS, and Bluetooth module. This box was then strapped and taped to the flat cross beam behind the athlete.

3.1.2 GPS

A GPS module was included with the IMU package on the boat. This provided speed, position, and heading of the boat. The Ultimate GPS module by Adafruit was chosen due to its relatively high GPS data output rate of 10 Hz. Accuracy of speed is specified as ± 0.1 m/s and known position to < 3 m[21]. The speed accuracy is satisfactory, however, it was unknown if the rapid boat speed changes during a paddle stroke would be observed by the GPS. An acceleration test was conducted and found that the GPS was able to obtain expected high velocity changes within the manufacturer's quoted accuracy. See details on this test in Appendix B.

3.1.3 Load Cell

Using a 6-axis load cell offers the advantage of obtaining a full force profile and determining the CoP. The mini58 6-axis load cell from ATI Industrial Automation Inc. (Apex, NC, USA) is rated IP/68 (10 m water submersible) with internal silicon gauges [2]. The paddle undergoes relatively high bending moments so a high strength load cell was needed. The mini58 is factory calibrated up to 120 Nm and 2800 N. The load cell is amplified using a battery powered wireless transducer that sends data through

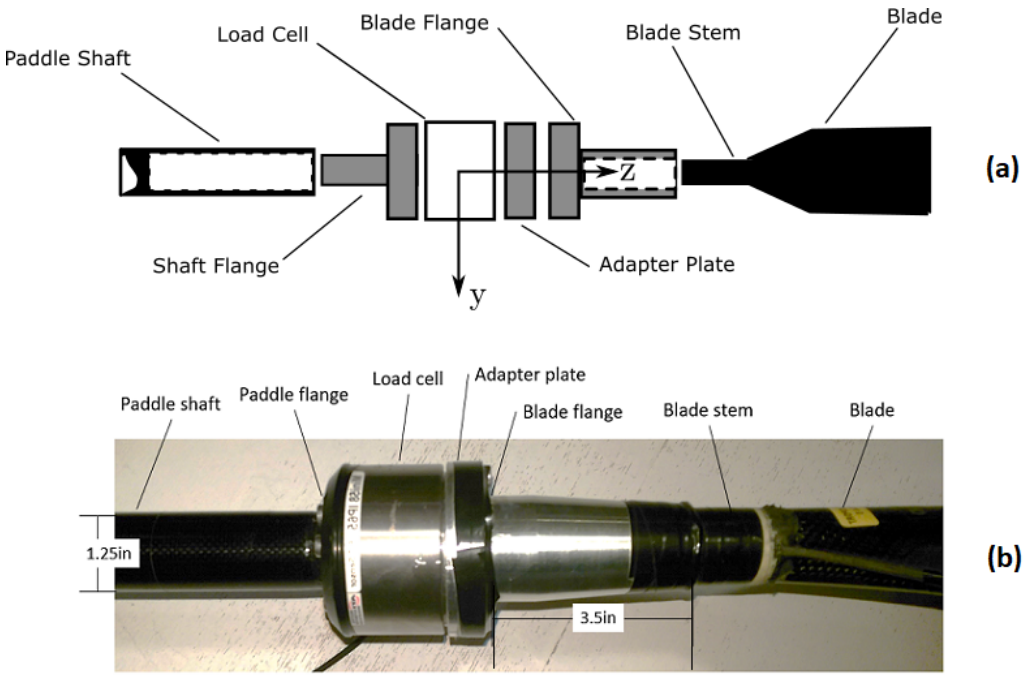

Figure 3.4: (a) An exploded-view drawing of the coupler system, not to scale. The load cell's x direction is coming out of the page, which is parallel to the normal of the blade's front face. **(b)** Close up image of the load cell attached to the paddle with the coupler system.

a network and can also internally log data. The wireless system was able to send the data at 75 Hz to the coach computer which processed, logged, and displayed the data in real-time.

Coupler System

This load cell type allows a full force profile to be known wherever it is placed. To be closest to the blade as possible, the load cell was placed at the intersection of the blade and the shaft of the paddle. One major design component of this system was the shaft-load cell coupler, shown in Figure 3.4. The load cell has a fixed bolt pattern on each side. The paddle, supplied by Braca Sports, comes in two parts (blade and paddle shaft). The system had to couple the load cell to the carbon paddle shaft and the carbon blade stem. In terms of design criteria, the coupler had to be: lightweight to not interfere with stroke style ($< 500\,\mathrm{g}$) and small enough to fit in-between the blade and the athletes bottom hand.

The three-piece 6061 aluminum coupler system was fabricated using a manual lathe and mill. The coupler system comprises of two flanges to fit to the paddle shaft and

Figure 3.5: Photo of the load cell system attached to the Braca paddle and blade, along with the wireless transducer.

blade shaft and one adapter plate. This plate was required so that the shaft would not interfere with the bolt pattern on the load cell.

The shaft-side flange is a 'plug' that internally inserts into the shaft, allowing the part to not interfere with the athletes hand. The blade-side flange fits on the outside of the blade stem, reducing deflection and ensuring the flange would not fail under the high bending moments. Stainless steel bolts are used in each of the three pieces to attach one to the other. Weight reduction techniques during manufacturing reduced the coupler weight by using tapers and chamfers in areas where excess material was not necessary. The resulting system can be seen in Figure 3.5.

Additional Load Cell Capability

The load cell is capable of determining the centre of pressure, or the effective force location of a simply supported beam. For example, say the load cell is in a fixed position with a long rigid beam fixed to its sensor face. An arbitrary force P pressing normal to the beam at distance d to the load cell would create a torque $T = Pd$. The load cell would then measure T and P, leaving d easily solved. This approach is used for the 6-axis load cell in the paddle. Determining this location from the load cell is simply

$$d = \frac{T_y}{F_x} \tag{3.1}$$

where T_y and F_x are the measured torque and force about the y and x axis respectively. The load cell is placed such that the x axis is normal to the blade face, where a force on the back face results in positive F_x readings. The y axis is lateral to the paddle shaft and the z axis points along the direction of the blade's chord line, as in Figure

3.4.

Load Cell Accuracy

Bench loading was performed with the load cell placed into the paddle to ensure the accuracy of the readings. A simply supported loading scheme was performed where a variety of weights (10 to 30 lbs) were applied to the bottom hand location and supported at the handle and on the back blade face. The uncertainty readings were: $F \pm 0.42$ N and $T \pm 0.55$ Nm. See more details on the loading test in Appendix B.

3.1.4 Combining Devices

Some measurements will require the merging data of two or more devices. The time domain relied on the devices' internal clocks that were synchronized using the laptop's time stamp. Due to differing output rates, data points were linearly interpolated so that all devices share the same time domain.

3.2 Ergonomic Considerations

The load cell is semi-wireless, meaning only one wire comes from the load cell to the battery powered wireless transducer that was clipped to the athlete's waistband. The other battery powered components (two IMUs and GPS) communicated wirelessly using Bluetooth. The system was designed to be modular, such that any Braca Sport blade could be inserted into the load cell coupler. This implies that an athlete could use the blade type with which he or she is most comfortable. The shaft used was shortened to accommodate the load cell's added length and is adjustable by 5 cm.

It was important to utilize the instruments in a manner that would not interfere with the athlete's performance. The load cell weighs 800 g, which is roughly the same weight as the paddle. This was a major concern, so the remaining materials, including the coupler system, were designed to minimize weight as much as possible. The athlete practiced with the system prior to recording data. He stated that the system did not hinder technical performance but the added weight increased the fatigue rate.

Paddle	
Model	Uni Extra Wide
Length	168 cm*
Total mass	760 g
Blade width	24 cm
Blade length	50 cm
Athlete	
Height	188 cm
Weight	86.2 kg
Canoe	
Model	Nelo C1 Quattro XL
Length	5.2 m
Beam	0.44 m

*Extendable up to 5 cm.

Table 3.1: Characteristics of the athlete and equipment used for the on-water measurements.

3.3 On-water Test Setup

The athlete used for the on-water measurements was an experienced sprint canoeist that paddled for the Canadian National Team. See Table 3.1 for details on the athlete and equipment used.

Immediately before the instrumented system was implemented on the water, a number of checks were performed. The IMUs were calibrated (using the procedure in Appendix A) and the orientation values were statically checked. The load cell was loaded with 20 lbs in a manner similar to the loading tests described in Section 3.1.3. The same test was performed after the on-water trial to evaluate for consistency which agreed within 5% of each other. The GPS and IMU units were secured to their appropriate positions using tape and zip ties.

These measurements were completed at the Mississauga Canoe club (located on Credit River) using an experienced national-level canoeist on a calm day. After the athlete warmed up, measurements of a variety of stroke types, or techniques, were recorded. Each test was separated by an appropriate rest period and included qualitative notes by the athlete as to which technique was used.

The goal of this test was to perform and measure a variety of strokes and techniques so that an evaluation of stroke comparisons could be performed. The on-water test

needed to confirm that the instrumentation system could differentiate stroke techniques by a variety of performance measures. These measures will be presented and described in the following chapter.

Chapter 4

Results & Discussion

The on-water data will be presented, analyzed, and discussed in this chapter. Raw data will be presented followed by a deeper analysis. The results will be related to past research and new findings will be explored. A number of different stroke types, or techniques, were performed compare performance. These different techniques are shown in Table 4.1. While described as *techniques*, it should be noted that different techniques inherently arise from different race paces. For example, a 1000 m pace will have different stroke rate and force profile to a 200 m sprint. In this case, the sprint technique presented here is the maximum output capacity for the athlete to achieve top speed. The steering, short, and long strokes were paced at 1000 m. Each test was kept under 45 s in duration so that fatigue was minimized and consistency remained through each test. A rest period between each set was also allotted.

4.1 Sample Data Analysis - 1000m Race Pace

To display the capability of the instrumented system, a small portion of the raw data results will be shown using three strokes of the first 1000 m race pace. This test set was paced very well; the average speed was within 6.4% of the C1 1000 m winning pace in the 2016 Olympic games [29].

4.1.1 Raw Data Results

This section will present the raw data from all sensors on the boat and paddle. Raw data in this context means the sensor's intended measurement values (e.g. load cell

Name	Duration (s)	Rest Period (s)	Description
50% power	30	105	Athlete utilizes 50% of maximum power output
Short strokes	21	27	Relatively shorter length of blade travel per stroke
Long strokes	27	106	Relatively longer length of blade travel per stroke
1000m race pace I	28	44	A pace set to a race distance of 1000 m
1000m race pace II	29	66	Additional pace set to a race distance of 1000 m
Sprint start	13	117	A pace set to a race distance of 200 m
75% power	25	-	Athlete utilizes 75% of maximum power output

Table 4.1: The list of test sets (i.e. technique types) that were performed and recorded.

force, IMU orientation). In later sections, the sensor's data will be merged together to obtain more information.

From the load cell forces in Figure 4.1 a stroke force profile can be described. The blade begins its downward descent towards the water at roughly 0.25 s. A small positive force on F_x is seen while the athlete sets up to begin the stroke where the blade enters the water at about 0.5 s. A sudden, sharp increase is seen until peak force is achieved. The time from blade entry to peak force is about 0.15 s. The draw phase then commences where a decrease in force is seen followed by a plateau. The exit phase starts where the sharp decrease in force begins at 1 s. The exit and or recovery may include steering as the blade comes out of the water and begins its ascent towards its setup position at 1.5 s. This description of phases seen in the first stroke of Figure 4.1 is shown and summarized in Figure 4.2 and Table 4.2.

It is often assumed that the force is normal to the chord line (i.e. blade surface) [36]. The forces seen in Figure 4.1 are minimal in the lateral (F_y) and longitudinal (F_z) directions, and are most likely due to buoyancy effects on the blade, except for the small peak in the positive directions during peak force. This small F_y and F_z peak

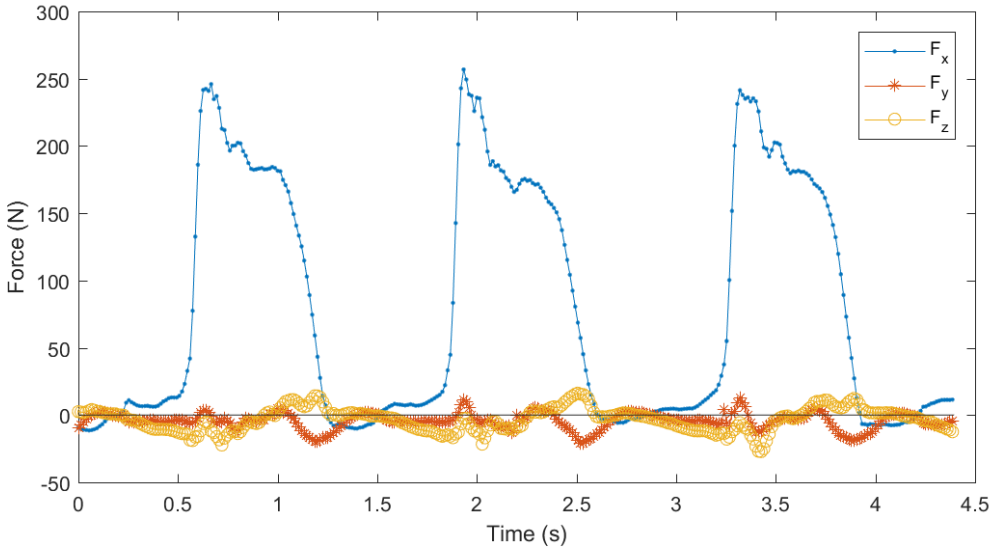

Figure 4.1: The load cell force data from a three-stroke portion of the 1000 m race pace test.

during peak F_x likely has hydrodynamic implications as blade speed (or blade slip) at this point is entirely in the forward-aft plane. However, the magnitude is small compared to F_x (less than 10%). A more relatively significant force in the lateral and longitudinal directions is observed later during the exit phase due to lateral velocity of the blade pulling out of the water. Therefore, given the minimal amount of in-stroke forces for F_y and F_z, it can be safely assumed that blade force is normal to the blade surface and that F_x is equivalent to the blade force F_B.

Numerous figures will follow to display the other available raw data of the same three strokes as in Figure 4.1. Torque data are shown in Figure 4.3. The torque about the lateral axis (y-axis) of the load cell is a result of the bending in the paddle due to the blade force F_B. Note that the T_y and F_x curves shapes are very similar but not identical; this is due to the changing centre of pressure (CoP) that will be discussed in-depth later.

Orientation data for the paddle are displayed in Figure 4.4. The plots of acceleration, angular velocity, and magnetic flux density data from the paddle's IMU can be found in Appendix B. The orientation of the boat is shown in Figure 4.5. Note that for presentation purposes, the yaw (ϕ) was averaged and zeroed for the three-stroke interval, since ϕ refers to the direction of travel to north and is often non-zero. Unfortunately, due to improper magnetometer calibration, the ϕ from the boat's yaw reading IMU

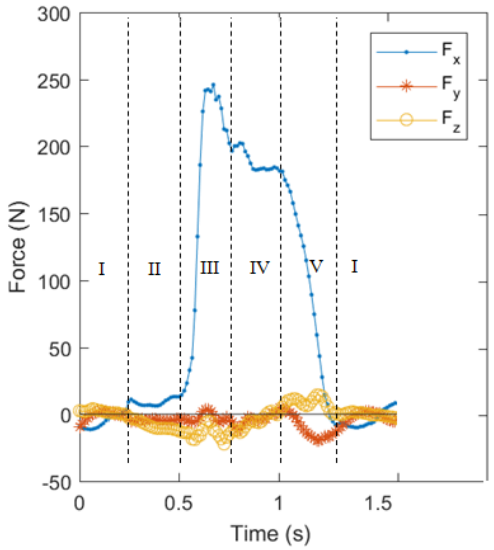

Figure 4.2: The load cell force data of one stroke of the 1000 m race pace test with phases.

	Phase	Start (s)	End (s)	Duration (s)
I	Recovery	0	0.25	0.25
II	Setup	0.25	0.5	0.25
III	Catch	0.5	0.7	0.2
IV	Draw	0.7	1	0.3
V	Exit	1	1.25	0.25

Table 4.2: The breakdown of the stroke phases from the left-side figure.

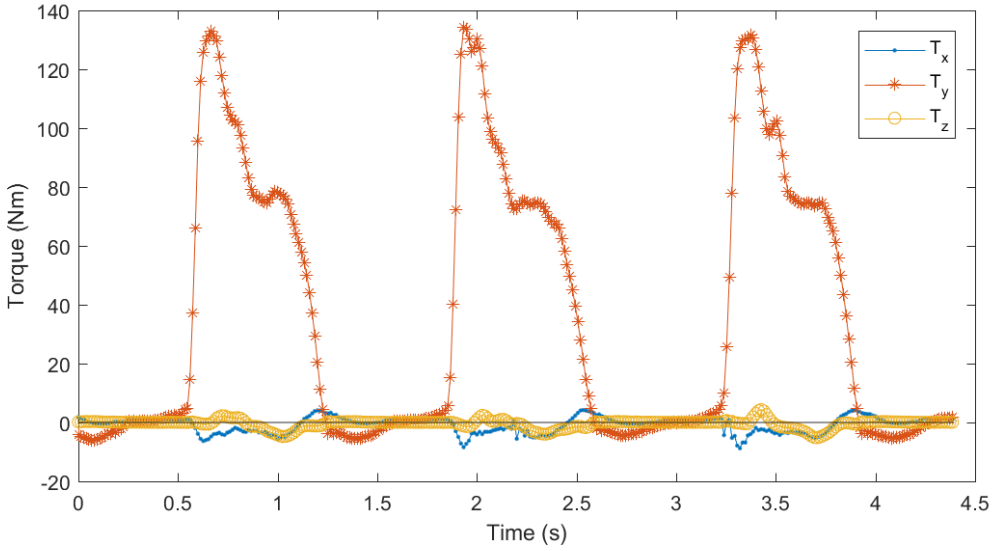

Figure 4.3: The load cell torque data from the 1000 m race pace test.

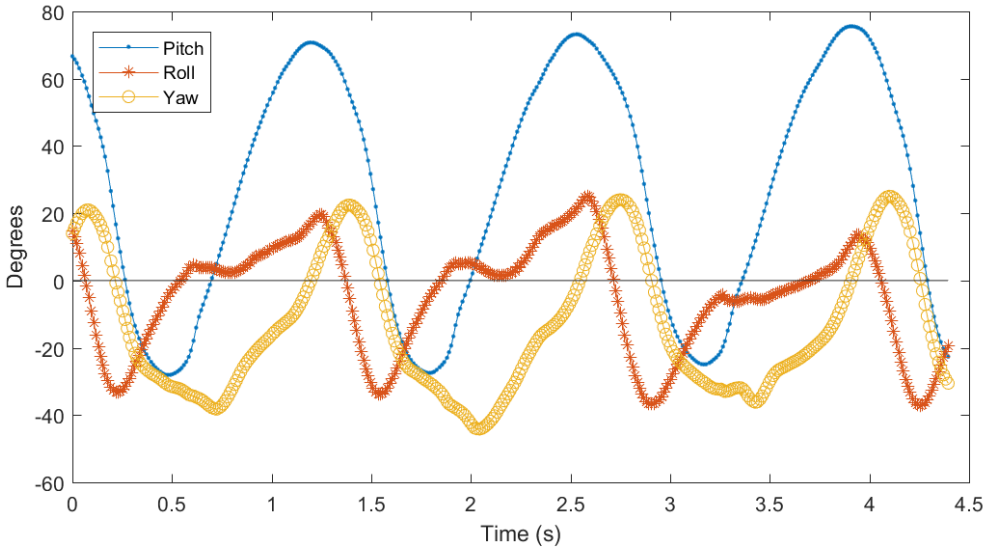

Figure 4.4: The pitch, roll, and yaw orientation data from the paddle's IMU during the 1000m pace test.

incurred some drift. Thus, the heading from the GPS is used.

The speed of the canoe from the GPS is displayed in Figure 4.6. This is plotted with F_x to show where the strokes are occurring. The speed is minimal as the blade enters the water and increases as soon as force is applied. In this example, a speed quirk occurs in strokes two and three during the boats acceleration. Shortly after peak blade force is achieved, the boat's acceleration becomes nearly zero. It is also apparent that a lower top speed was achieved in these strokes than the first stroke without this quirk. One speculation for this is that the motion of athlete could have slowed the relative speed of the boat.

The speed profile contrasts to rowing where there is a decreasing velocity for a short period after the catch phase [38]. This in-stroke decreasing velocity was explained by mainly three criteria:

- the oar blades must be moving faster than the relative water velocity
- the blade force must first overcome water resistance
- the motion of the rowers slow the shell relative to the water.

These criteria are not necessarily true, as it has been more recently shown that lift forces on the rowing blade, while it is moving slower than the water, contribute to

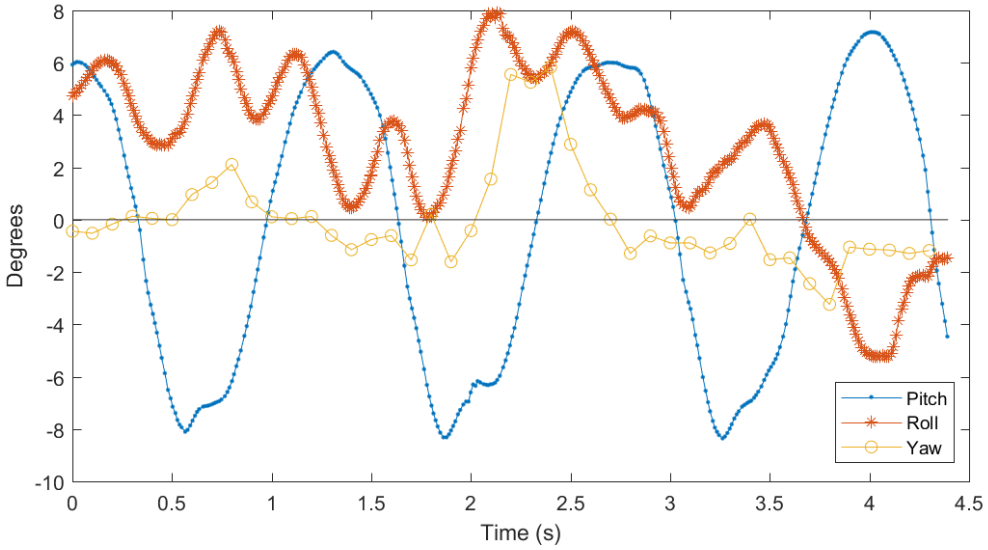

Figure 4.5: The pitch, roll, and yaw orientation data from the boat's IMU during the 1000 m race pace test.

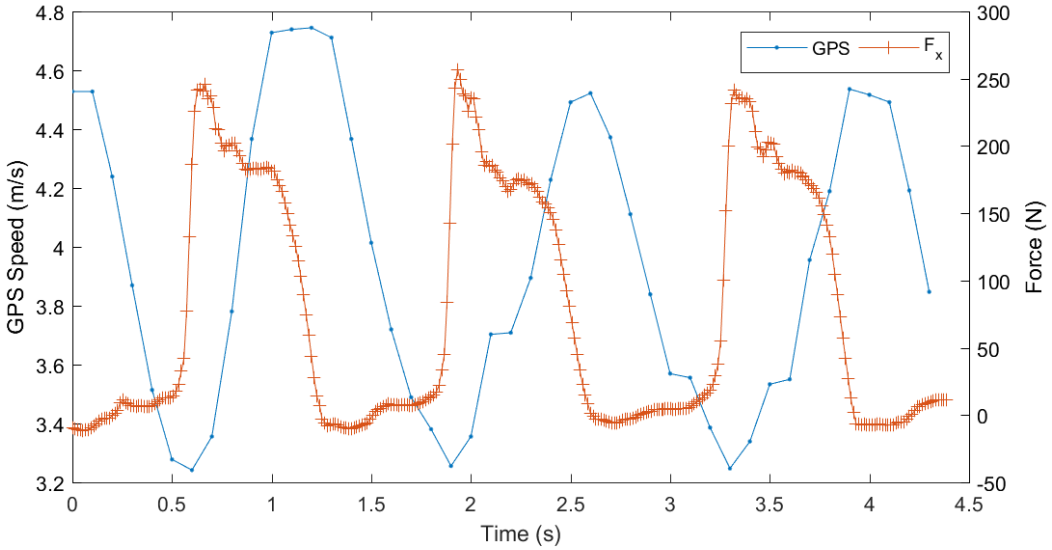

Figure 4.6: The GPS speed of the canoe boat shown with F_x of the load cell during the 1000 m race pace test.

propulsion forces [55]. In the canoe's case no significant delay in canoe speed increase is seen after the catch phase. The halting forward motion of the athlete's trunk at the end of the setup phase may help to increase the relative boat velocity. Something to note is that the speed only rapidly increases after the peak blade force. Velocity increases to its maximum during the exit phase, then decreases again until the next stroke cycle.

Boat Acceleration

The boat's inertial acceleration is found using a rotation matrix using the IMU's orientation. This puts the IMU's acceleration readings, which are

$$A_{xyz} = \begin{bmatrix} a_x \\ a_y \\ a_z \end{bmatrix}$$

into an inertial, or ground, frame of reference. This is,

$$A_I = \begin{bmatrix} a_P \\ a_S \\ a_V \end{bmatrix}$$

where a_P is forward (i.e. propulsive), a_S is side, and a_V is vertical acceleration. The rotation process uses the boat orientation angles as

$$A_I = R_z(\psi)R_y(\theta)R_x(\phi)A_{xyz} \tag{4.1}$$

where rotation matrix R is the matrix used to perform the rotation about the specified axis. These are defined as follows:

$$R_z(\psi) = \begin{bmatrix} \cos\psi & -\sin\psi & 0 \\ \sin\psi & \cos\psi & 0 \\ 0 & 0 & 1 \end{bmatrix} \tag{4.2}$$

$$R_y(\theta) = \begin{bmatrix} \cos\theta & 0 & \sin\theta \\ 0 & 1 & 0 \\ -\sin\theta & 0 & \cos\theta \end{bmatrix} \tag{4.3}$$

$$R_x(\phi) = \begin{bmatrix} 0 & 0 & 1 \\ 0 & \cos\phi & -\sin\phi \\ 0 & \sin\phi & \cos\phi \end{bmatrix} \tag{4.4}$$

The A_I results are found in Figure 4.7. The forward acceleration a_P appears to have a

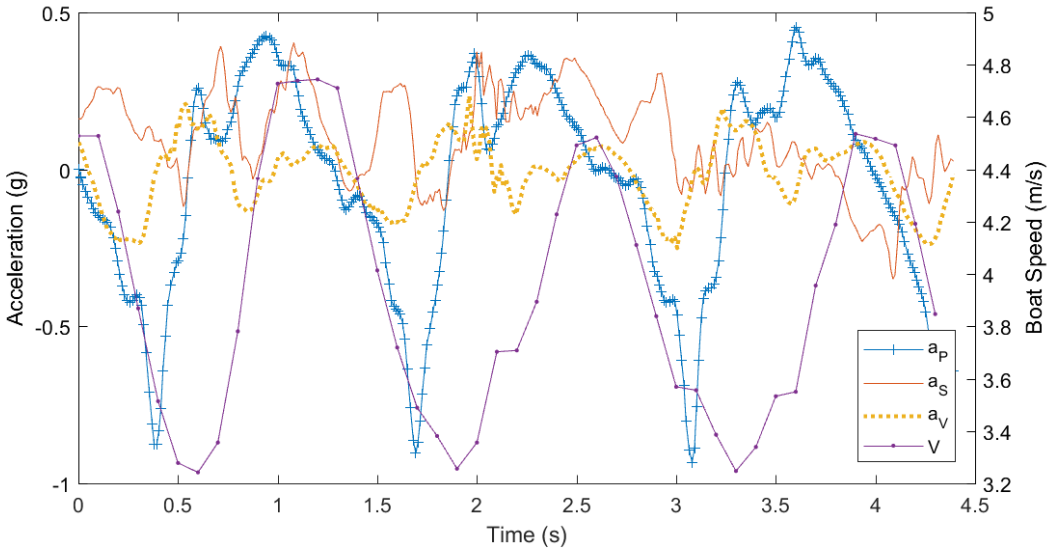

Figure 4.7: The forward (propulsive) a_P, side a_S, and vertical a_V boat inertial accelerations during the 1000 m pace test. The accelerations are smoothed using a moving average function with a span of 3. Canoe velocity V from the GPS is included as reference.

consistent dual positive peak during the catch–early drive phase. The first positive peak and its following dip at the catch is likely due to the athlete's body motion. The more prominent and maximal peak (about 0.4 to 0.5 g) occurs closer to the top speed of the stroke during the drive phase. This agrees well with accelerometer data from another C-1 canoe [16]. The acceleration become negative at the end of the exit phase where it then quickly, and briefly, decreases to -0.9 g. Acceleration a_P does not directly match with the lower time resolution readings of the GPS velocity V. Some discrepancy is likely due to cross-talk from the placement of the IMU on the boat, as it was not practical to place it on the centre of rotation. This can be seen for the side acceleration a_S, which is expected to be small since there is little canoe motion occurring in that direction. The deceivingly high results are due to the IMU's placement above the roll centre of the canoe.

The boat dynamics are not the focus of this thesis. However, canoe velocity will

later be used to determine a drag profile of the canoe. The raw data presented thus far has given plenty of information, most athletes and coaches would be satisfied to conclude their performance findings from it. Stroke rate, force profile, boat speed, and blade angles give enough information to roughly track an athlete's training and performance. It is here where an in-depth analysis of the data will be performed to determine details such as blade force components and power, and how some parameters can be misleading.

4.1.2 Data Merge and Analysis

Much more insightful information can be determined through an investigation of the raw data. From here, analyses will be done by comparing device data across the test sets and/or fusing data of the multiple devices.

List of Assumptions

The assumptions used to simplify the mechanics are:

- paddle shaft is rigid
- negligible blade buoyancy
- work done by athlete during blade-in-air is negligible
- only surge (forward) motion of the canoe
- forces due to blade accelerations are neglected

Centre of Pressure

Force across the blade face is not uniform [43]. The load cell is not able to determine a force gradient; it can only determine the integrated forces normal to its axes. By combining the force and torque data an equivalent force location can be determined using the three-point bending scheme. This value represents the centre of all the non-uniform forces that act on the blade. To do this, an assumption is made that the blade force F_B is centred and normal to the blade's chord line, which is acceptable knowing the blade is symmetrical and there are minimal F_y and F_z forces. When the

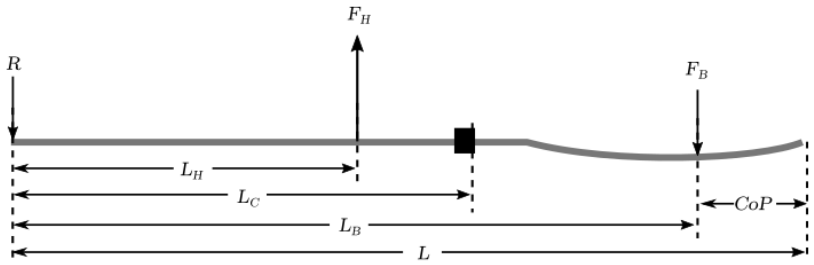

Figure 4.8: The paddle free body diagram as a three point loading. Handle reaction force R (top hand) is the length reference for the bottom hand force F_H at L_H, the load cell readings at L_C, and the location of the blade force F_B at L_C. The CoP is equal to the difference of paddle length L and L_B.

paddle is taken as a three-point force diagram as in Figure 4.8, the blade force F_B acts at the CoP, or length L_B from the handle.

This location is the combination of all forces applied to the blade and is determined by the equation

$$L_B - L_C = \frac{T_y}{F_x} \tag{4.5}$$

where T_y and F_x are the torque and force readings of the load cell. The CoP is then easily found by

$$\text{CoP} = L - (L_B - L_C) \tag{4.6}$$

with an example of these readings from the 1000 m pace test shown in Figure 4.9.

The results show that as the blade enters the water and the force is developed, the location rapidly approaches the tip of the blade to within 5 cm. The peak force corresponds to where the force is closest to the tip of the blade. As the force decreases, the CoP moves closer to the centre of the blade, about 15 - 20 cm from the tip. The force is closest to the centre of the blade while the force profile is in its plateau region, which is nearing the end of the draw phase. After this, the force begins to decrease and the CoP moves toward the tip of the blade again as it leaves the water.

Figure 4.10 shows the blade used in the tests is shown with dimensions. The CoP moves from 5 to 20 cm while the geometrical centre of the blade is 22.5 cm from the tip. This means that the bulk force location on the blade does not, for this case, occur on the geometrical centre of the blade. What also is of interest is the blade force peaks while it is closest to the tip of the blade. As the draw phase develops, the force moves

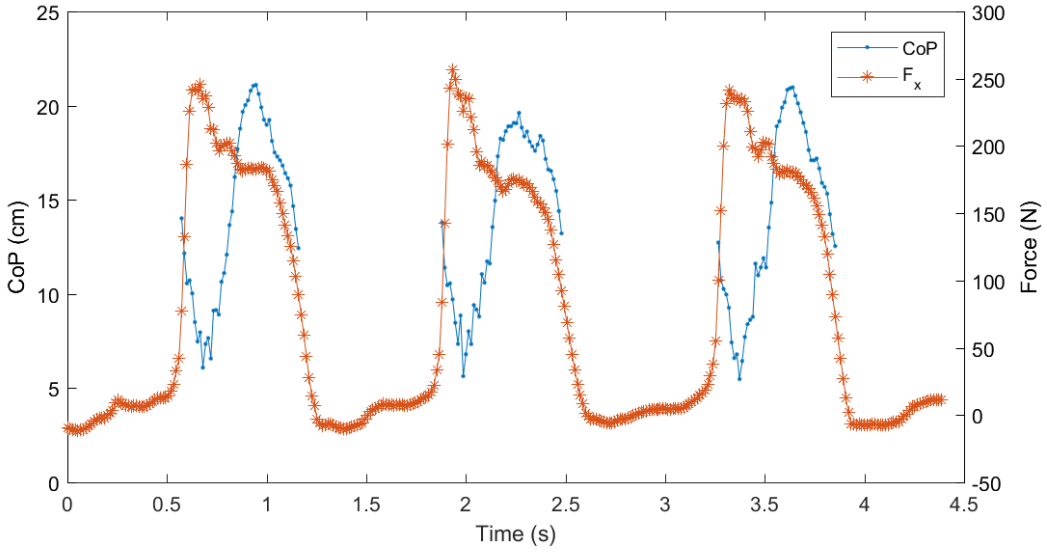

Figure 4.9: The centre of pressure of the force on the blade. The amount refers to the distance away from the blade tip. This is displayed with F_x of the load cell during the 1000 m race pace test.

towards the centre of the blade but stops short by a few centimetres. The transition from the draw phase to the exit phase shows the force location moving back towards the tip as the blade leaves the water.

This is contrary to the CFD finding of Campbell Ritchie and Selamat [11], where the CoP occurs 49% of the distance from the blade stem to the blade tip. This differing result is due to their conditions: the blade is stationary and the water velocity is only applied normal to the blade. However, the CoP motion here agrees with the dynamic blade motion CFD result of Morgoch [43].

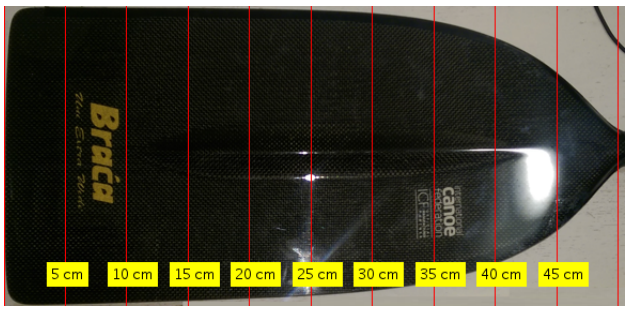

Figure 4.10: The blade face used in the on-water test, scale is shown to compliment the CoP data from Figure 4.9.

This is information provides a potential improvement for the common assumption to place the CoP at the geometrical centre of the blade [12, 35]. It would be more appropriate to assume that the force occurs at the mid point of the maximum and minimum CoP. From Figure 4.9, the mid point is approximately 12.5 cm. If a force location must be assumed, an approximation of 25% of the distance from the tip to the neck of the blade is more appropriate. This assumption still produces an inaccurate force profile, as the following will show.

Force Location Implications

An example of assuming a fixed CoP will help illustrate what the CoP means in terms of the measured force. A discrepancy arises if the blade force is assumed at a fixed position, denoted as L_{Beq}, because the load cell's readings would not complete the mechanics of the moment diagram, as in Figure 4.11. This discrepancy is solved by assuming a force F_f exists at another arbitrary fixed location L_f. The 'fictitious' torque/moment M_f is found by

$$M_f = T_y - F_x(L_f - L_c) \tag{4.7}$$

where L_c is the load cell location. The equivalent blade force F_{Beq} at the fixed location can then be found with

$$F_{Beq} = \frac{M_f}{L_{Beq} - L_f} \tag{4.8}$$

while F_f can be found by a force balance.

The locations of equivalent and fictitious forces are rather arbitrary, as in they can be selected by assumptions. As discussed previously, it is common to assume that the geometrical centre of the blade face (22.5 cm from tip) is the CoP of the blade force. However, as it was seen in Figure 4.9, the CoP does not reach the geometrical centre of the blade. Knowing that the CoP remains roughly between 5 - 20 cm from the blade tip, we could let L_{Beq} be 12.5 cm, the midpoint of the CoP range. From this, the results of the equivalent and fictitious forces are shown in Figure 4.12. Note that L_f is assumed to be halfway between L_{Beq} and the neck of the blade, this is assumed due to the likelihood of adverse forces on the top portion of the blade [43].

This shows that if a fixed CoP is assumed, there are forces elsewhere on the blade that can be considered adverse and beneficial propulsion forces. F_f in Figure 4.12 is

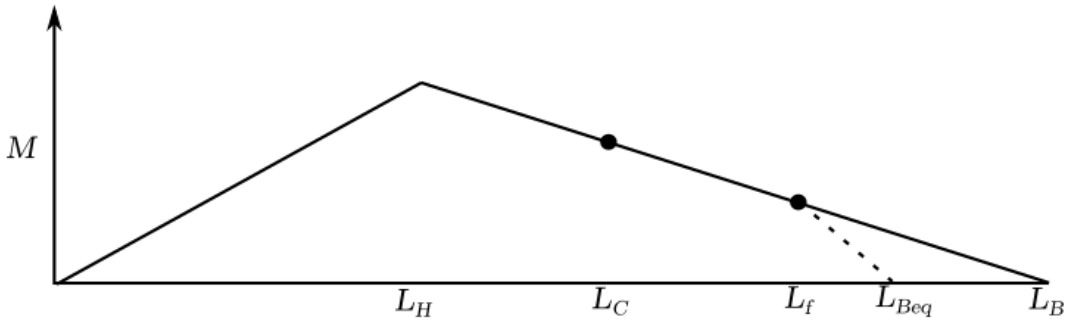

Figure 4.11: An example of a moment (M) diagram along the paddle length. An equivalent blade force F_{Beq} at fixed location L_{Beq} is resolved by a 'fictitious' force F_f (obtained from M_f) at a fixed location L_f. Real blade force acting on the centre of pressure would continue on the straight line moment curve and occur at L_B.

assumed to be parallel in direction to the true blade force F_B, indicating that small adverse forces could exist in this manner. However, if large adverse forces did exist, the measured CoP would appear to be far past the blade tip. Since the CoP remains between the middle and tip of the blade, the adverse forces, if they exist, must be relatively small. It could be argued that the CoP remains near the tip during the late-catch/early-draw phases due to adverse forces, however, its extent remains unknown. F_B is shown in the figure as reference, where a significant magnitude difference can be seen. This illustrates the importance of knowing where forces on the blade actually exist and obtaining true blade force.

Force Components

Blade force in an inertial reference frame (i.e. the boat's frame) is valuable information as it can tell which direction the blade is pushing the boat. This will break down the components into propulsive, vertical, and side forces. These force components are compiled using a similar rotation matrix to Equation 4.1, except now using the paddle's orientation angles and the load cell force readings. These inertial vector forces F_I are defined as

$$F_I = \begin{bmatrix} F_P \\ F_S \\ F_V \end{bmatrix} \tag{4.9}$$

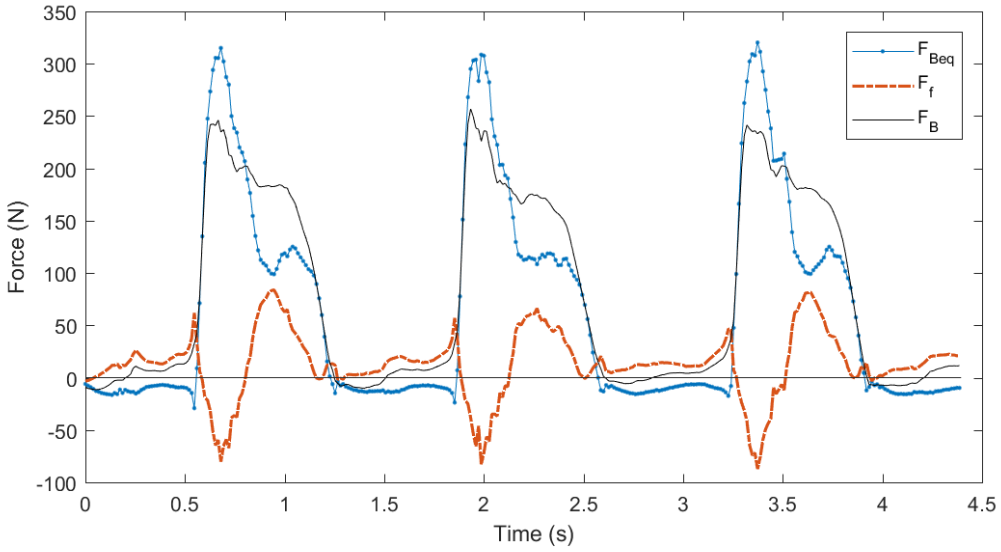

Figure 4.12: The equivalent F_{Beq} and fictitious force F_f from assuming a fixed CoP location L_{Beq} at the midpoint of the known CoP range. L_f is assumed to be halfway between the geometrical blade centre and the blade neck. Measured F_B included as reference.

where F_P, F_S, and F_V are the propulsive, side, and vertical forces respectively. These forces are found by

$$F_I = R_z(\psi)R_y(\theta)R_x(\phi)F_{xyz} \tag{4.10}$$

where F_{xyz} are the load cell readings in vector form. From this, the propulsion ratio of blade force can be found using the definition in Equation 2.1, such that

$$\eta_{force} = \frac{F_P}{F_B} \tag{4.11}$$

which is shown in Figure 4.13 along with all the inertial components and blade force. It can be seen that the force propulsion ratio η_{force} remains high (nearly 1.0) through the entry and catch phases, meaning the force is practically all propulsive. The ratio drops steadily after the peak force in the draw phase to ~ 0.35 at the exit. This is due to the increasing pitch angle of the paddle as it sweeps through the stroke. During the exit phase, as the force goes to zero, the ratio rapidly rises which is likely due to steering or buoyancy effects of the blade.

There is a considerable amount of F_V at the end of the draw phase due to the paddle's shallow angle to the water. This intuitively implies that a large portion of the athlete's effort is sinking the boat into the water. This act also likely increases

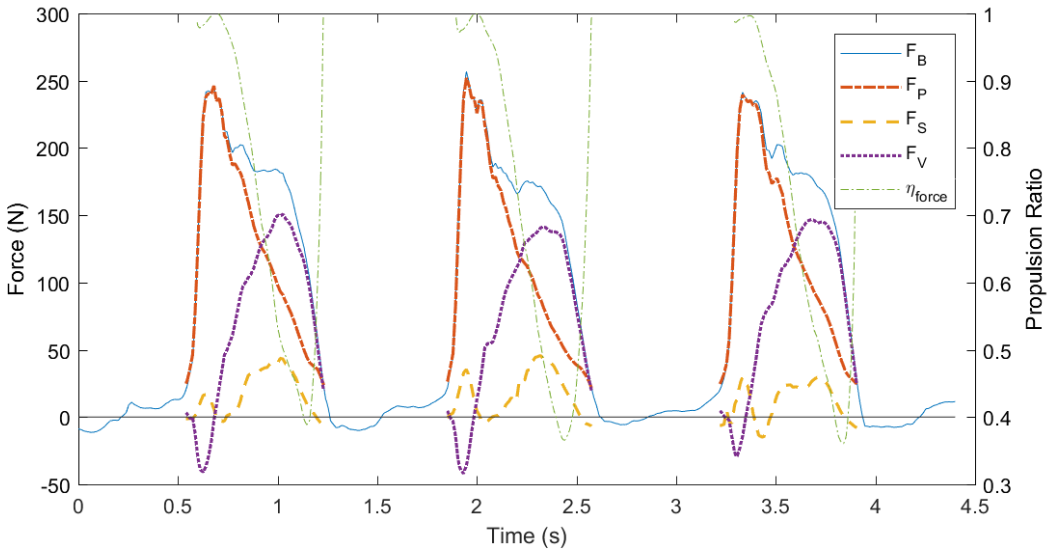

Figure 4.13: The blade force with its propulsive, side, and vertical components during the 1000 m pace test. Blade force F_B and propulsion ratio η_{force} are also included.

drag since the boat's wet surface area A_w increases. From this, it would seem that keeping shorter strokes would lead to an overall better performance since less effort would be wasted in the vertical plane. However, the blade's shallow angle to water is necessary for steering and the recovery process. An adjustment of technique that can rectify these issues has potential to reduce this wasted effort.

There are numerous ways that have been presented in literature to calculate the efficiency of a stroke (see earlier Section 2.3.1, also Cabrera and Ruina [10] and Macrossan and Macrossan [36] for good reviews of determining rowing efficiency). The intuitive approach of efficiency is the instantaneous ratio η_{force} which has been used in rowing [36, 56]. In rowing, it is likely that the most efficient part of the stroke is the early-catch where the blade is not yet at 90° to the direction of the water flow. This efficiency gain comes from the high lift forces that contribute to the forward propulsion force [56], resulting in a high propulsion ratio. In canoeing, the forces are overwhelmingly normal to the blade, thus the propulsion ratio remains a good indication the blade's contribution to propulsion force.

The ratio does not consider the overall magnitudes of force. This means there is little benefit of a high ratio if the forces are small. To help to rectify this, an average

ratio $\bar{\eta}$ using the time integral of propulsive and total force can be computed. This is,

$$\bar{\eta} = \frac{\int F_P dt}{\int F_B dt} \tag{4.12}$$

which is equivalent to the propulsive impulse over the total blade impulse. This was completed over a number of strokes of the differing techniques, the results can be found later in Table 4.5.

4.2 Stroke Profiles of Differing Techniques

A comparison of stroke techniques can now be done. Parameters can be explored to find which one results in a best estimate of performance. A simple comparison of force profile can be observed of each technique, such as in Figure 4.14. Most techniques have a peak force when the blade is first fully immersed. The force decreases, then some techniques have a 'plateau' where the force remains relatively constant during the drive phase. The force then steadily and quickly decreases throughout the exit phase as the blade leaves the water.

Noting the differences between the sprint technique and the 1000 m provides a practical contrast as these techniques are true race paces. The force profiles share a number of similarities; peak force occurs during the late-catch phase followed by a lower plateau region during the draw phase. The sprint pace had a 50% greater force peak and 0.161 s less time of blade-in-water. Another relevant fact is that the overall average canoe speed of the sprint phase was 7% faster.

In Figure 4.15 three contrasting stroke types are compared: 50% power, 1000 m pace, and sprint pace. Here, the differences of blade force F_B, stroke rate, and the canoe velocity V can be clearly seen. The sprint case has a much higher peak force, though this peak is very brief and returns to a profile similar to the 1000 m. The 50% power profile is longer in length but has a much lower force average. Three stroke cycles are completed in 5.5 s for the 50% case, while six are completed in the sprint case in the same time frame. The sprint's velocity profile is much more sporadic than the 50% power and 1000 m cases. The velocity usually begins to rapidly rise during the drive phase when the blade is fully buried. The sprint case, however, has a seemingly inconsistent velocity profile. In more than one of strokes, the velocity continues to rise during the exit phase of the stroke. It is likely that this is due to the more rapid

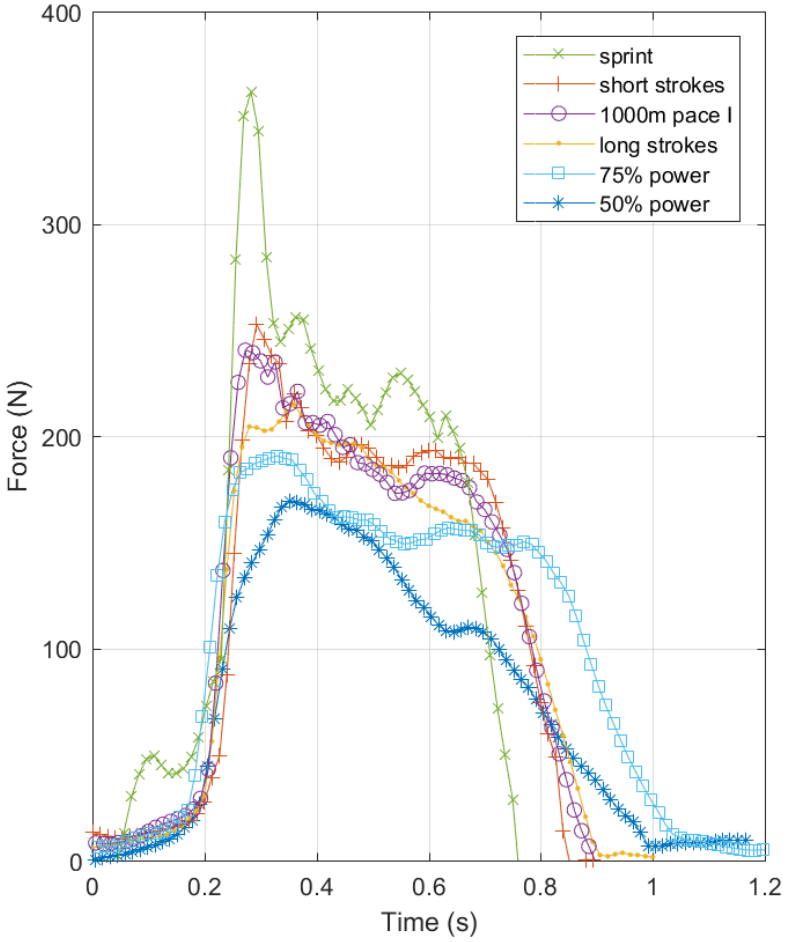

Figure 4.14: Comparison of the a typical stroke from the six main tests sets. The strokes were visually synchronized by aligning the catch and the peak force.

body motion that is required to achieve the high stroke rate. This body motion causes the boat to surge forwards and backwards through the stroke, while maintaining an overall net-zero canoe velocity change.

A comparison of CoP trends can be done to determine if the force acts differently through each technique. As seen in Figure 4.16 there is little difference between each technique. All of the techniques operate very similarly during the catch and draw phases, where the CoP moves from near the tip 5 - 10 cm to 17 - 21 cm from the tip. It should be made clear that the CoP does not reach to the geometrical centre of the blade (22.5 cm) for any of the techniques. Because the CoP is very consistent across

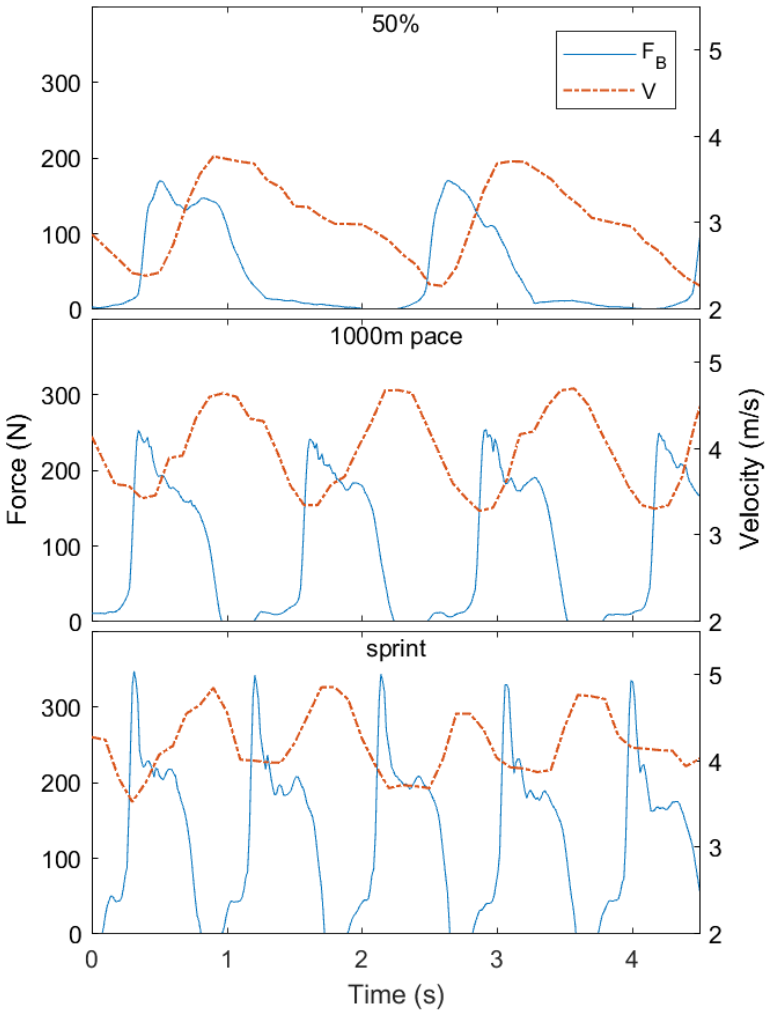

Figure 4.15: Force and forward canoe velocity of three contrasting stroke types/techniques. The 50% power case is the slowest with lowest stroke rate, the sprint race pace has the highest speed with fastest stroke rate.

the stroke types, it may be appropriate to model the CoP motion instead of assuming a fixed CoP for the less sophisticated instrumentation setups.

4.3 Boat Drag Analysis

In order to calculate an efficiency that is based on blade force and the corresponding canoe velocity, the effort required to drive the boat (i.e. boat drag) needs to be quantified. In particular, how this effort varies with the canoe velocity needs to be

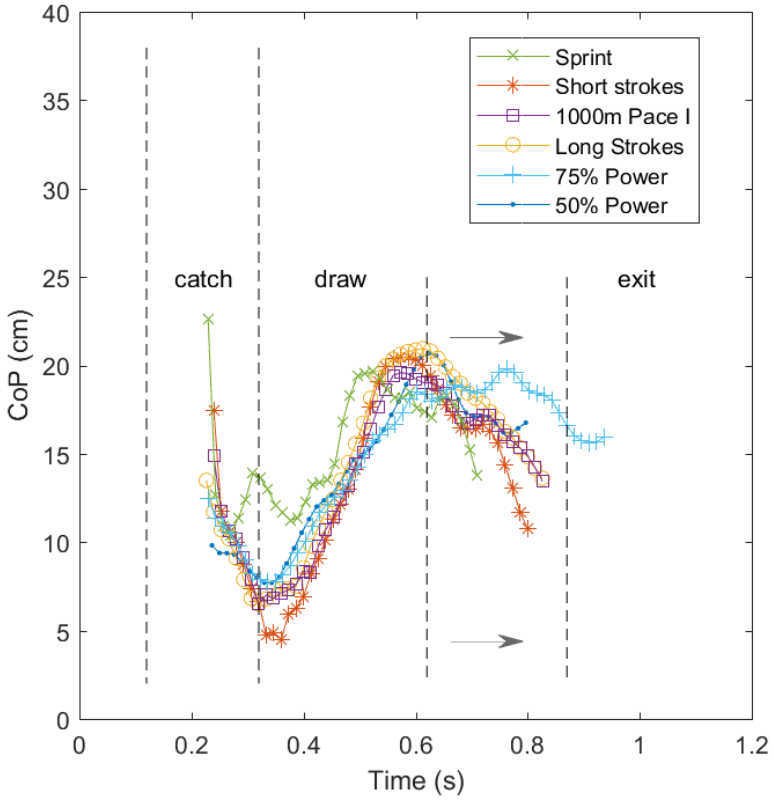

Figure 4.16: A comparison of the CoP of each technique observed in the on-water trial. One typical stroke was selected from each technique, data were smoothed using a moving average of a span of 3 and displayed with a F_B threshold of 70 N. The approximate phases are marked, though each technique has unique phase timing, the varying start of the exit phase is noted by the region with arrows.

determined. This section will determine a deceleration trend due to the drag on the canoe, which will indicate the minimum drag profile of the canoe. This calculated drag will be due to friction, pressure (form), and wave drag of the boat in the water and any air resistance as well. It has been stated by Seiler [54] that boat surface drag accounts for 80% of the total drag, while wave and air resistance share the remaining 20%. Robinson et al. [51] states that skin friction accounts for approximately 80% and wave 20% of total drag. Another analysis by Jackson [32] found the breakdown as follows; friction drag 72%, air drag 7%, and wave drag as 21% for a K1 canoe of an unspecified model at 4.83 m/s. The drag presented here will explore a total drag coefficient C_T but will neglect all motions of the athlete and boat except for forward

velocity. This enables an estimation to the minimum boat drag which disregards other drag due to heaving, pitching, and yawing.

Four trials were taken, two trials each of up and down the natural flow of the river. The athlete was asked to reach top speed then allow boat to drift down to minimum speed. The athlete's motion was minimized during speed data acquisition to minimize accelerations and pitching of the canoe during the coast-down period. The captured top speed reached nearly 4.5 m/s and the minimum speed was roughly 2 m/s. Real top speed surpassed 5 m/s; however, athlete motion voided these measurements. If the canoe went any slower the athlete lost stability and risked capsizing.

The drag on the boat F_D is unknown, however, the velocity profile of the decelerating boat is known. Using the general drag equation,

$$F_D = ma = -\frac{1}{2} C_{Ti} \rho V^2 A_w \tag{4.13}$$

where C_{Ti} is the total drag coefficient, the relationship of velocity, the drag force, and the constants can be estimated using the known velocity profile and some numerical methods. These three methods will be compared with previously derived boat drag profiles of similar hulls.

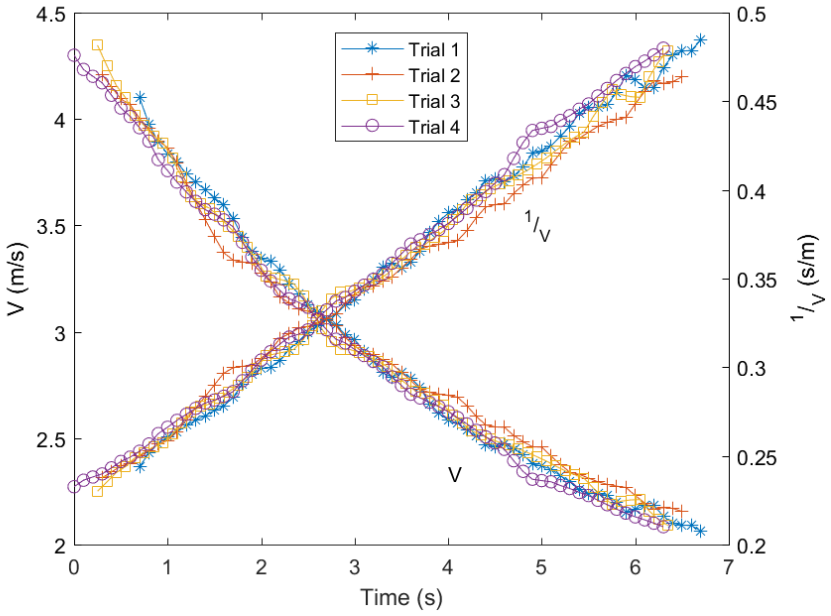

Figure 4.17: The boat velocity V and inverse velocity $1/V$ of the four coast-down trials.

Characteristic	
Mass m	105.9 kg
Beam B	0.44 m
Length l	5.2 m
Wet area A_w	2.25 m^2

Table 4.3: Characteristics of the C1 Quattro XL canoe used to determine the drag.

A few boat characteristics must be determined, which can be found in Table 4.3. Wet surface area A_w was estimated using the waterline and a simplified planform of the hull. Similarly shaped K1 Vanquish LI and LII kayaks have a A_w of 2.22 and 2.34 m^2 respectively [37]. Mass m includes the weight of the equipment and athlete.

4.3.1 Method I

One simple approach, which is dubbed as Method I, uses the central difference numerical solution of dV/dt and solving for the remaining constants, including the total drag constant C_T. The result is a noisy collection of data points, which when bulk averaged, results in a C_{T_I} of 0.0038 ± 0.0005. In addition, the trends of the C_{T_I} with V are not the same across the trials. Trials 1 and 4 have a slightly decreasing C_{T_I} with increasing boat velocity. This is contrary to trial 3, which is nearly constant, and trial 2, which has a slightly increasing C_{T_I}. The coefficient C_T is sensitive to dV/dt which leads to the noisy and differing trend. There are a number of possible explanations for trial 2's increasing C_{T_I} such as boat wake, excess boat roll, serge, or inadvertent paddle drag.

4.3.2 Method II

Since C_T is highly sensitive to the variation of V, a more appropriate way to determine it may be to integrate over time intervals of 0.7 s across each of the trials. This would be taken as

$$\int_{V_1}^{V_2} V^{-2} dV = \frac{\rho A_w}{2m} \int_{t_1}^{t_2} C_{T_{II}} dt \tag{4.14}$$

where V_1 and V_2 are the boat velocities between a local time interval t_1 and t_2. Since the $\rho A_w/2m$ term can be determined using the boat characteristics, only the $C_{T_{II}}$ needs be solved, which is the slope of the linear slope of the plot of $1/V$ and t as in Figure 4.17. This method essentially smooths the noise seen from the direct numerical

solution of dV/dt. By averaging local slope intervals of each of the trials, the average $C_{T_{II}}$ was determined to be 0.0038 ± 0.0002. This method agrees well with method I and appears to have less uncertainty.

4.3.3 Method III

Since C_T is a variable that is technically based on boat velocity, another approach can let it be based on some constant coefficient C_k and boat velocity V such that

$$C_{T_{III}} = C_k V^k \tag{4.15}$$

This can be substituted into the general drag equation 4.13 and linearized as

$$\ln\left(-\frac{dV}{dt}\right) = \ln\left(\frac{C_k \rho A_w}{2m}\right) + (2+k)\ln V \tag{4.16}$$

The $\ln(dV/dt)$ term, determined using 2^{nd} order central difference scheme, and $\ln V$ can be compared to obtain the slope, which is equivalent to the $(2+k)$ coefficient. All four trials resulted in a mean and standard deviation of $(k+2) = 1.84 \pm 0.23$. This results in the remainder of the equation to be

$$\ln\left(\frac{C_k \rho A_w}{2m}\right) = -3.13 \pm 0.33$$

Solving for $C_k = 0.0040 \pm 0.001$, the $C_{T_{III}}$ can now be determined at various velocities. At $V = 4\,\text{m/s}$, $C_{T_{III}} = 0.00326 \pm 0.0009$ which also agrees well with methods I and II.

4.3.4 Drag Force Discussion

An accurate drag model is difficult to solve for many boats and hulls. Previously developed models with similar hull shapes can be compared to the introduced methods in the previous section. The International Towing Tank Conference (ITTC) adopted a method of determining ship hull resistance by using extrapolation of scaled models [42]. This approach uses a scaled model with the Froude number ($Fr = u/\sqrt{gl_o}$) remaining the same as the full-scale ship while assuming that the friction and form drag forces scale with the appropriate Reynolds numbers.

Parameter	Series 64 range	Sprint canoe
Length to displacement ratio $l/\nabla^{1/3}$	$8 - 12.4$	11
Froude Fr	$0.06 - 0.55$	0.57
Block coefficient $C_B = \nabla/LBT$	$0.35 - 0.55$	0.5
Beam to draft ratio B/T	$2 - 4$	3

Table 4.4: Testing range of various parameters of "Series 64" hulls, found in Molland et al. [42], with the corresponding sprint canoe value. Estimated sprint canoe values are comparable to similar C-1 canoe hulls found in Bugalski [9].

The total drag C_T is found by

$$C_T = (1 + k_f)C_F + C_R \tag{4.17}$$

where the $(1 + k_f)$ term is a form factor, C_F is the friction drag coefficient, and C_R is the residual wave making resistance coefficient. The three-dimensional ITTC 1957 model-ship correlation line is

$$C_F = \frac{0.075}{(\log_{10} Re_l - 2)^2} \tag{4.18}$$

where $Re_l = 2.1(10)^7$ for the canoe (Reynolds hull length number $Re_l = Vl/\nu$ at $4\,\mathrm{m/s}$). Coefficient C_F is then calculated to as 0.00265.

The form factor depends on the hull shape and can range from $(1 + k_f) = 1.03$ to 1.3 for typical vessels. Couser gives a relationship for narrow bilge hulls that are similar shaped to the sprint canoe hulls [42]:

$$1 + k_f = 2.76(\frac{l}{\nabla^{(1/3)}})^{-0.4} \tag{4.19}$$

The sprint canoe displacement, determined from total mass, is $\nabla = 0.1059\,\mathrm{m}^3$. This gives $(1 + k_f) = 1.058$. This agrees well with longer rowing shell values of 1.02 to 1.04 [47].

Wave resistance is also hull shape dependent and usually determined through tow tank testing. Yeh tested a set of "Series 64" hulls in a range of parameters which are also similar to the sprint canoe, seen in Table 4.4 [42]. Yeh found that the length to displacement ratio was by far the most significant of the parameters.

Interpolation of the Yeh data gives $C_R = 0.00095 \pm 0.00001$ at $V = 4\,\mathrm{m/s}, Fr =$

0.55. Uncertainty is based on a simple sensitivity of the C_B and B/T values and approximation of hull shape. For $V = 3.19\,\text{m/s}$ and $Fr = 0.45$, $C_R = 0.00105 \pm 0.00010$.

With C_R, the combined value of an estimated drag at $V = 4\,\text{m/s}$ can be determined from Equation 4.17, where $C_T = 0.00376 \pm 0.00050$. This result agrees very well with the previous methods derived from the boat velocity data. Note that this drag does not include air drag, which would increase the drag 7 to 10%, as discussed previously. With extrapolation, this C_T falls within a range that is agreeable with the derived methods. It is expected that C_T varies with V, so a check of this trend should be done. From Equation 4.18 for a Re_l range of $1.0(10)^7$ to $2.1(10)^7$ (i.e. V is $2\,\text{m/s}$ to $4\,\text{m/s}$), C_F can be approximated as proportional to $V^{-0.16}$. This aligns well with what was found as coefficient k for $C_{T_{III}}$.

It is clear that all three of the derived drag coefficients are similar to each other and agree with the hull drag from literature. This supports the justification of using a drag profile in the canoe's energy dissipation, which will be presented later in this thesis.

While the drag estimates presented here appear to fit the physics very well, it should be noted that these values may not resemble real race drag. The collection of velocity data was taken after the athlete stopped paddling and allowed the boat to drift down to minimum speed. It did not include any additional or reduction of drag due to pitching, heaving, and rolling which may change results considerably. It remains an open question as to the level of effect that these neglected movements have on total drag during a race.

4.3.5 Velocity Fluctuations

The topic of canoe velocity fluctuations causing reduced efficiency was explored by Martin and Bernfield [38]. Higher velocity gives greater drag force and lower speeds requires more energy to bring the mass to the average velocity. The greater this range, or amplitude, of the velocity the greater the inefficiency of the boat. From this theory, the authors concluded that a lower variance of speed should result in higher overall efficiency, however, their experimental results yielded no significant relationship. However, it has been more recently suggested that reducing fluctuations is a sign of better performance [59]. Negative but weak trends were observed with the on-water GPS data by fitting average velocity vs. amplitude ($r^2 = 0.385$) and the root-mean-square deviation (RMSD) ($r^2 = 0.202$) of each technique.

It may be better to analyze the velocity distribution and skewness of each stroke type. If positively skewed, the peak of the distribution will be lower than the mean. This means the canoe is spending more time in low velocity, thus less drag acts on the canoe. However, this obviously means the canoe is covering less distance. Shown in Figure 4.18, it can be seen that the sprint technique has a more positive skew than the 1000 m pace, and a much different distribution to the 50% power case, which has a negative skew. The skew values, which are presented in Table 4.5, had a strong positive linear trend ($r^2 = 0.952$) with the average velocity of the corresponding technique.

These trends are not necessarily a sign of performance, but rather a function of canoe velocity and stroke rate. As canoe velocity rises, the drag force rises $\propto V^2$, as the general drag equation shows. This means the canoe will decelerate faster at higher speeds, thus it is more likely the canoe will be seen travelling at the lower-end of the speed distribution. The slower techniques, such as the 50%, are negatively skewed likely because the athlete's power input is relatively lower compared to the drag. This implies that the 50% power case is more energy efficient than the sprint case. Tracking skew has the potential to give an athlete how their strokes compare to others in terms of velocity profile and net speed and stroke type.

4.4 Calculating Efficiency

Understanding efficiency, as described in Section 2.3.1, is crucial for it tells the athlete what amount of input work is actually used to propel the boat forward. However, efficiency does not equate performance. A slow stroke can be have nearly perfect efficiency, though in sprint canoe, slow and steady doesn't win the race. In order to determine an efficiency in terms of work, a value of power into the water must first be estimated.

4.4.1 Power

Ergometers are often measured in power units as a base for performance, but this measurement is unknown for on-water trials. With all things being equal, more power means a faster canoe. Having an in-lab ergometer performance indicator comparable to on-water results would be a significant advantage. Power into the water P is calculated

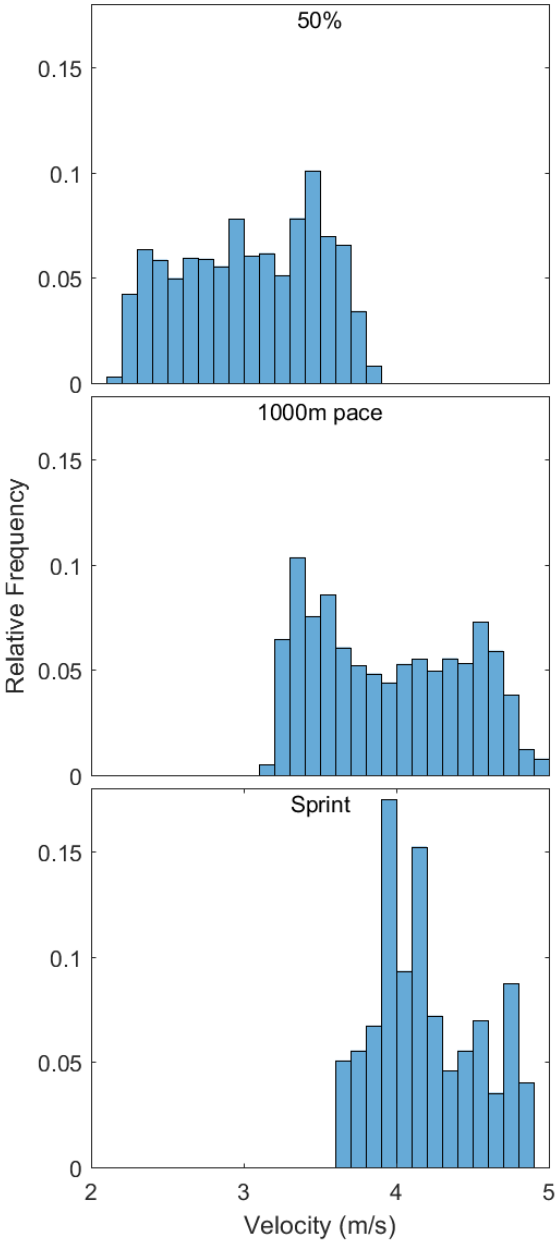

Figure 4.18: The relative frequency of the velocity samples of three differing stroke types.

using

$$P = F_B v_B \tag{4.20}$$

where F_B is the total force on the blade and v_B is the blade velocity. This velocity term is an estimate since true blade velocity is not obtainable with the current measurement setup. In reality, the blade has varying velocity across the chord line relative to the water. A short discussion on this can be found in Appendix C. To simplify this, the velocity is taken as the athlete's perspective, where the blade's centre of pressure (CoP) is moving towards the aft. This is found using

$$v_B = \omega L_B \tag{4.21}$$

where ω is the pitch angular velocity of the paddle ($\omega = d\theta/dt$), and L_B is the distance from the paddle's handle to the CoP. Using the pitch angular velocity assumes that the top hand is a fixed pivot point relative to the boat, as in Figure 4.19. This is

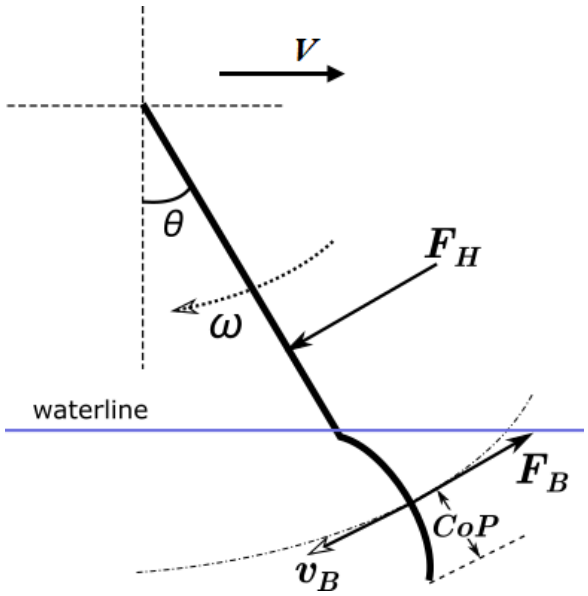

Figure 4.19: Definition of v_B as if it moves along with respect to the athlete's fixed top hand position. With this, when viewed from the boat, the top paddle handle is stationary. When viewed from the ground, the handle moves with the canoe at V.

justified by seeing that there is a small amount horizontal motion of the top hand through a stroke (see Figure 1.2). Note that this P is also equivalent to

$$P = F_H v_H \tag{4.22}$$

where F_H is the bottom hand force and v_H is the hand velocity. It should be stressed that this is a velocity estimation in lieu of having no instantaneous blade path or the athlete's exact pull-path. Propulsive power P_P is

$$P_P = F_P \omega L_B \cos(\theta) \tag{4.23}$$

The results are shown in Figure 4.20 along with its propulsive power ratio η_P given by

$$\eta_{power} = \frac{P_P}{P} = (\eta_{force}) \cos\theta \tag{4.24}$$

The power profiles are similar to the force profiles in that the peak occurs at the front-end of the stroke, where the blade is just fully buried, then decreases with a short 'plateau' region. The peak propulsion ratio occurs just after peak power then quickly reduces as the stroke continues.

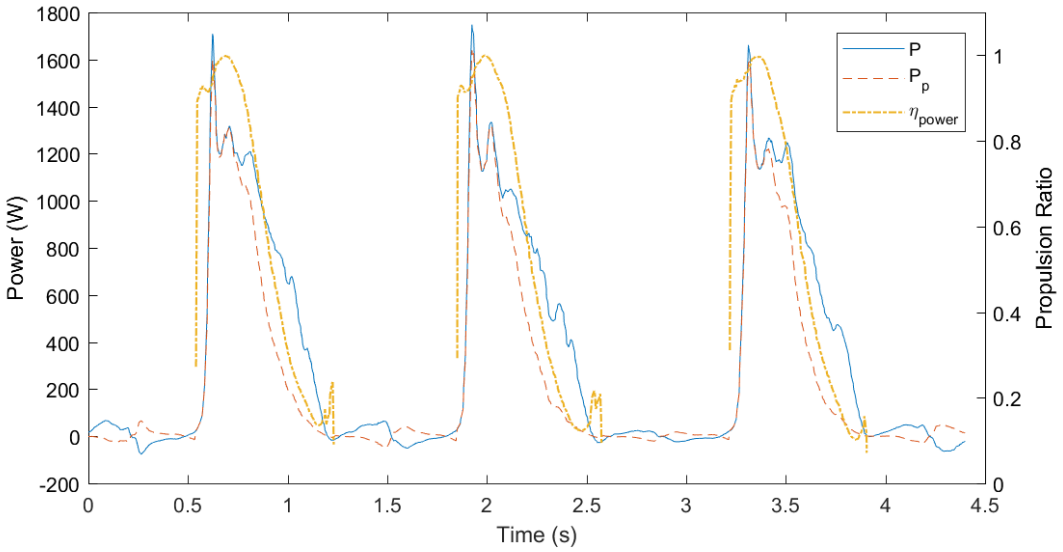

Figure 4.20: Power P, propulsive power P_p, and propulsive power ratio η_P during the 1000 m pace test.

4.4.2 Work Efficiency

Drawing inspiration from previously derived efficiencies from Section 2.3.1, a new parameter is introduced that incorporates efficiency with high performance. This encompasses the total energy expended, or work, over boat travel distance d_b, this is

then compared to the average speed during the interval. Energy expended, or work, into the water is,

$$E_{in} = \int P dt \tag{4.25}$$

where the interval can be over one or more stroke cycles. In this case, a number of strokes were selected from each technique, shown later in Table 4.5. The selected strokes disregarded the start and finish strokes using visual inspection of the velocity cycle of the stroke. In other words, only the strokes with relatively little change between the minimum and maximum velocity between stroke cycles were used. Taking E_{in}/d_b effectively calculates the amount of energy used by the athlete per meter of canoe distance. This is plotted with the average speed of the canoe during the sampled strokes, shown in Figure 4.21. A more efficient curve would be shifted to the right, where the same amount of energy expended results in the higher speed. Fortunately this can already be seen between three techniques; the 1000 m paces and short stroke techniques share very similar E_{in}/d_b at around 100 J/m. The 1000 m I test had the higher average speed with only spending 0.2% more energy in than the 1000 m pace II test. The athlete spent 4.4% more energy for short strokes with a negligible change in overall speed. The data are also presented later in Table 4.5.

This approach can be used for the boat's energy as well. An analysis of drag energy per unit distance travelled would give insight into how the kinetic energy is dissipated compared with hull velocity. From Equation 4.15 and 4.25, we can obtain

$$E_{Drag} = C \int V^{k+1} dt \tag{4.26}$$

where $k = 1.925$ and C, a combined drag coefficient, is 4.172. These were from a preliminary drag analysis, which used a power law regression fit of the velocity coast-down trials. While these coefficients are different than those found in Section 4.3, they still fall within the uncertainty. Taking this on a per unit distance E_{Drag}/d_b would indicate how efficiently the boat was travelling, however, the drag equation only accounts for minimum drag. Since the hull is the same for all the measured tests the E_{Drag}/d_b measurement is simply related to the velocity of the hull and its energy dissipation.

A combination of these terms can be used as an energy balance of the system. Energy is being spent by the athlete to propel the boat forward that is resisted by air, water, and wave drag. The work done by the athlete is not totally transferred

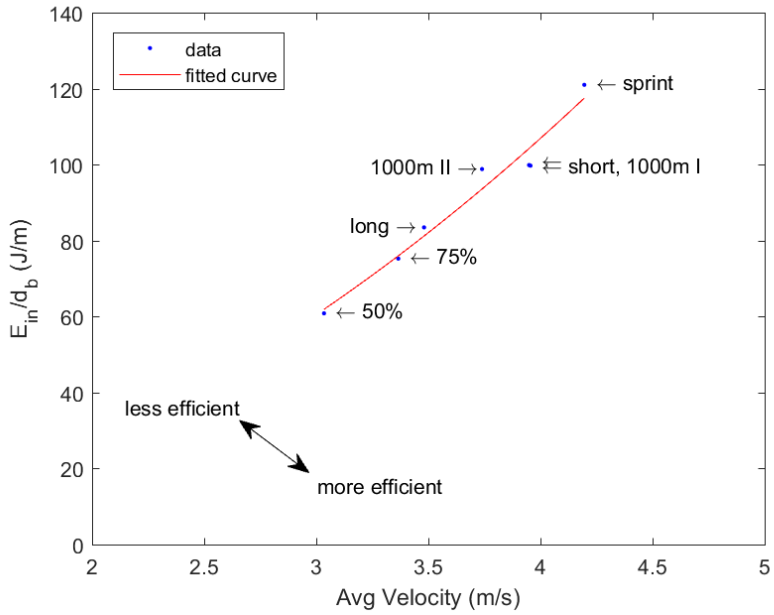

Figure 4.21: The total expended energy into the water by the athlete per meter of canoe distance plotted with the average speed of the canoe during the test interval. See Table 4.5 for data. (Fit: $y = 5.24x^{2.18}$, $r^2 = 0.956$)

into propulsion; sources of waste include forces that cause vertical motions, water hydrodynamics that cause no propulsion, or negative forces onto blade face. To isolate this, an efficiency can be developed that isolates work into the water by the athlete and the energy dissipated due to propulsion drag (minimum boat drag), simply

$$\epsilon = \frac{\text{output}}{\text{input}} = \frac{\text{minimum dissipated boat propulsion}}{\text{work into water}} \tag{4.27}$$

which is equivalent to

$$\epsilon_{energy} = \frac{E_{Drag}}{E_{in}} \tag{4.28}$$

This equation is calculable with the available on-water data over one or more stroke cycles.

4.4.3 Force Efficiency

Since blade velocity v_B is calculated by an approximation, another efficiency is proposed without its use. This uses average boat velocity $\overline{V}$ and average blade force $\overline{F_B}$ through

any number of stroke cycles. This equation is

$$\epsilon_{force} = \frac{\overline{V}^k}{\beta \overline{F_B}} \tag{4.29}$$

where β is the blade-in-water ratio (β = blade in water duration/total stroke duration). The $\overline{F_B}$ term is the calculated using only in-stroke values. In other words, all blade-in-air force values ($\approx 0\,\text{N}$) are ignored. The β term accounts for the time that the blade is not in the water, allowing for a more realistic representation of the force and stroke rate required to achieve the average speed. Coefficient $k = 1.925$ is again used to simulate the canoe's drag force which is proportional to V^k as previously discussed. The ϵ_{force} would be best used to compare stroke types as the units do not represent a true efficiency. The objective is for the athlete to obtain a higher value; higher average velocity with lower average force input.

4.4.4 Efficiency Implications

From analysis of the efficiency, energy expended, and propulsion ratio data, it appears that a shorter stroke within the 1000 m pace yields a higher canoe speed without too great of a cost of an inefficiency and higher fatigue. Between the technique types, efficiency tends to decrease as the average boat velocity increases (fit: $y = -0.10x + 0.97$, $r^2 = 0.586$). However, the short and 1000 m I stroke types were better performing outliers. In terms of efficiency and the resulting canoe velocity, it appears that the 1000 m I and short stroke cases were the best performing techniques.

Since there are two efficiency calculations present, it is important to investigate their comparability. The plot of the ϵ_{energy} vs. ϵ_{force} is shown in Figure 4.22. With a moderately strong fit of $r^2 = 0.705$, it can be said that these efficiencies are comparable but not identical. More on-water data is required to conclude which one serves a better purpose. Determining ϵ_{energy} is slightly more difficult to measure, as it includes an additional drag term and the blade velocity estimation. The ϵ_{force} includes one drag term, however, a drag estimation of $k = 1.78$ to 2.0 may be satisfactory as found in the Section 4.3.

The efficiency values of the on-water techniques of several strokes are presented later in Table 4.5 along with other parameters and metrics. The resulting ϵ_{energy} values (0.55 to 0.7) for sprint canoe are lower than rowing efficiencies found by previous research

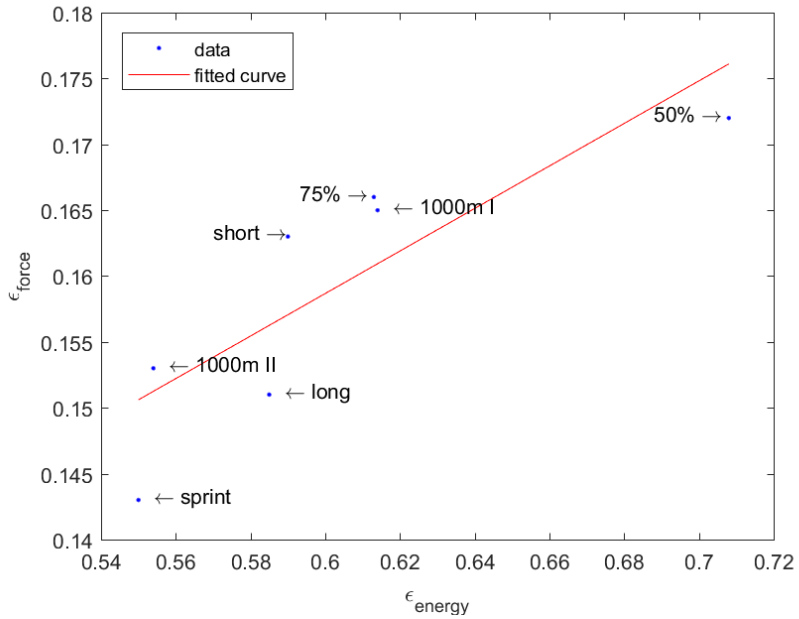

Figure 4.22: The ϵ_{energy} vs. ϵ_{force} of each technique with a linear fit to compare compatibility. See Table 4.5 for data. (Fit: $y = 0.161x + 0.0618$, $r^2 = 0.705$)

(0.7 to 0.85) [10]. This can be expected as the sport mechanics are not the same. These efficiencies were also analyzed with the root-mean-square deviation (RMSD) and amplitude of the canoe velocity as in Section 4.3.5, however, no significant relationship was found. Perhaps a larger sample size of strokes is required to obtain a strong trend but it appears that velocity amplitude is not a proper sign of performance. The velocity distribution skewness has a moderately strong correlation to the ϵ_{force} and ϵ_{energy} ($r^2 = 0.723$ and $r^2 = 0.696$ respectively). This supports the earlier postulation that the canoe's velocity is more positively skewed as the strokes become more inefficient. Again, this remains suggestion, as the collected data sample is too small to make definitive conclusions.

4.4.5 Paddle Elasticity

One aspect that is often overlooked is the mechanical effects of paddle shaft elasticity. As force is applied to the paddle the shaft bends that stores elastic energy. This energy releases as force application decreases. It is likely that paddle elasticity reduces overall efficiency because peak force occurs during peak propulsion ratio. In other words, the paddle stores the most elastic energy while the force application is perpendicular to the

water surface. As force application reduces, the released elastic energy is released into the vertical component. This adversely transfers energy from the propulsion component into the vertical component. This seemingly reduces efficiency, however to what extent is unknown. Two previous studies found that a flexible shaft produced a notable difference from rigid shaft assumptions [43, 57]. It is hopeful that the instrumented paddle will be capable of investigating the shaft stiffness effects in the near future.

4.5 Performance Parameters

The key parameters often used in literature will be compared from each test. Some of these include impulse, peak force, stroke rate, power, and efficiency. These are common parameters often used in literature to compare and analyze strokes of various water sports [18]. Table 4.5 shows common parameters between the test sets. Stroke cycles were determined by using a blade force threshold. The 'in-stroke' and 'out-of-stroke' portions were determined when $F_B > 20\,\mathrm{N}$ except in the sprint technique set where a threshold of 70 N was chosen. This was done to accommodate the greater forces in the sprint case during the recovery and setup phases from the paddle swinging faster through the air.

A careful look into the parameter results shows that the changes between each test are quite small. For starters, an important difference is the average speed. A higher speed of 6%, such as the difference between 1000 m I and II, may seem too small to note, however in race situations this is a major difference.

Impulse J_B of the blade force F_B is given by

$$J_B = \int F_B dt \tag{4.30}$$

and is solved of each stroke. It is often used as a performance parameter [46, 5], but it can be seen that the impulse hardly changes across stroke styles yet different canoe velocities are yielded. This indicates that impulse should be used in conjunction with stroke rate as stated by Baker [3], which would effectively determine the rate of impulse.

There is one inconsistency that arises from the data, which is the blade submerged percentage of the short vs. the long strokes. It was expected that the short strokes should have a smaller β since the blade leaves the water earlier. However, it appears

that the short stroke case had an overall longer time in the water but also had a much higher stroke rate. This implies that the long stroke case had both longer time in and out of water. This suggests that the athlete increased his stroke rate for short strokes without much adjustment of blade technique. Since a higher stroke rate generally leads to a faster canoe speed, a comparison of the short vs. long strokes in terms of stroke length and boat velocity outcome should not be done.

Average power and impulse (along with its stroke rate) remain, as expected, a good predictor of the average speed of the canoe. Efficiency appears to roughly decrease as canoe velocity increase, presumably to do inefficient motions expended to put more power into the water.

The $\bar{\eta}$ ratio appears to distinguish between the two 1000 m pace set pieces; 1000 m I is 0.775 and 1000 m II is 0.797. There is a clear increase in $\bar{\eta}$, suggesting an increase in efficiency for the second piece as more of the athlete force input is going toward boat propulsion. This $\bar{\eta}$ increase is the result a reduced vertical force while the propulsive force remained relatively constant. However, the average boat speed is 0.2 m/s less for the second piece, while one should again note that the two pieces have almost identical propulsive forces. Though, it is also true that the vertical blade forces affect boat speed (e.g. through increased boat drag). The reduction in boat speed, given almost identical propulsive force and improved $\bar{\eta}$, suggests that the propulsive to total force ratio, although worth having, is not the ideal measure of stroke efficiency.

4.6 Hydrodynamics

While it is not directly possible to analyze the hydrodynamics surrounding the blade using the instrumented system, comparisons can be drawn to confirm any findings. The decrease of propulsion at the late catch/early draw phase may be due to similar results [55] that rapidly increasing angle of attack of pitching airfoils at first creates an increased lifting force, followed by a sharp fast decrease [15].

The significant decrease of propulsion force during the late-catch phase due to the adverse pressure at the top portion of front blade face makes intuitive sense [43]. However, this decrease was not found. This means if the negative propulsive pressure exists, it is significantly smaller than past CFD results. A small portion could still be affecting F_B and decreasing the overall total blade force read by the load cell.

	50%	Short	Long	1000 m I	1000 m II	Sprint*	75%
number of strokes	10	5	5	10	10	4	7
duration (s)	19.08	6.05	7.34	12.97	13.02	3.74	12.34
strokes/minute	31.4	49.6	40.9	46.3	46.1	64.2	34.0
β (%)	47.0	55.6	51.8	54.0	55.5	58.0	45.5
d_b** (m)	57.6	23.9	25.5	51.3	48.5	15.5	41.0
d_b/stroke (m)	5.76	4.78	5.10	5.13	4.85	3.88	5.86
$\overline{V}$ (m/s)	3.04	3.95	3.48	3.95	3.73	4.19	3.37
SD	0.170	0.193	0.154	0.161	0.114	0.173	0.086
V variance (m/s)	0.197	0.228	0.245	0.244	0.227	0.109	0.275
V RMSD (m/s)	0.444	0.478	0.495	0.494	0.476	0.330	0.525
V skewness	-0.148	0.269	0.0852	0.199	0.219	0.428	−0.0195
V kurtosis	1.82	1.92	1.55	1.74	1.75	2.16	1.64
$\overline{F_B}$ (N)	105	156	141	158	149	190	137
SD	14.4	9.11	8.36	6.17	12.5	8.00	6.42
$\overline{F_B}$ peak (N)	168	245	216	250	257	337	192
SD	7.74	7.44	3.32	6.79	9.93	6.42	10.3
$\overline{t_{F_B}}$† (s)	0.18	0.122	0.17	0.125	0.114	0.0675	0.18
SD	0.028	0.035	0.047	0.041	0.119	0.0096	0.044
$\overline{P}$ (W)	467	852	650	821	746	953	627
SD	45.2	64.1	50.1	51.9	60.8	39.9	24.2
$\overline{J_B}$ (Ns)	93.5	105	107	112	108	104.6	110
SD	3.69	7.06	7.47	1.79	6.00	5.28	6.09
$\bar{\eta}$	0.776	0.858	0.734	0.775	0.797	0.744	0.808
E_{in}/d_b (J/m)	52.9	103.9	83.0	99.7	99.4	120.6	75.2
E_{Drag}/d_b (J/m)	37.5	61.3	48.5	61.2	55.0	67.1	46.1
ϵ_{energy}	0.708	0.590	0.585	0.614	0.554	0.55	0.613
ϵ_{force}	0.172	0.163	0.151	0.165	0.153	0.143	0.166

* Different stroke threshold used, see text for details.
** d_b: total forward boat distance travelled.
† t_{F_B}: Average time to peak blade force (F_B).

Table 4.5: A comparison of various parameters for the different techniques tested. Data was collected over a number of strokes after steady canoe velocity was achieved. The averages are calculated on a per-stroke cycle basis, then averaged again over the number of sampled strokes. The standard deviation (SD) is the deviation of each stroke's average.

Chapter 5

Conclusions & Recommendations

This instrumented system was the first detailed measurement of sprint canoe forces. Previous blade instrumentation has been very limited and required significant assumptions to resolve the measurements. It was common practice to only acquire single component bending shaft strain, which required a fixed centre of pressure assumption to obtain blade force. In addition, the lack of paddle orientation omitted the possibility of properly obtaining blade force in the boat's frame of reference. The instrumented canoe and paddle showed that these assumptions cause a significant difference of true propulsive blade force.

The Braca Sport paddle, fitted with the 6-axis load cell and 9-DOF IMU, was able to capture 3-axis of inertial force and torque. The IMU, which provided paddle orientation, enabled the analysis of which direction the force was applied throughout the stroke. The resolved propulsion, vertical, and side components allowed an indication as to how and where the athlete applied the force. The IMU and GPS placed on the canoe boat also tracked orientation and speed. All data from the sensors were streamed wirelessly to a coach boat laptop which was able to track performance in real-time.

Based on these measurements, various assessments of efficiency were developed. Using coast-down trials of the canoe, a drag force profile was derived using three different methods. This was compared with the input blade force and input work to determine an output/input efficiency. The proposed efficiency calculation was inspired by both past research and the available data of the instrumented system. This included a blade efficiency value ϵ and an energy expended per unit distance E_{in}/d_b. The proposed efficiency and performance indicators are likely to be useful tools in training

and coaching, as they can predict canoe speed and athlete fatigue.

5.1 Results Summary

An on-water test was completed with the athlete performing seven differing stroke techniques that allowed a comparison of a range of stroke types. Commonly used performance parameters used in sprint canoe were presented, such as stroke rate, stroke distance, and peak force. In addition, more complicated measures such as efficiency evaluations, velocity fluctuations, work, impulse, and power were presented.

One finding to note was that the load cell confirmed that the forces remain largely normal to the blade face throughout a stroke. There are some tangential (F_y) and compression/tension (F_z) forces throughout the stroke, however, these are negligible compared to the normal force (F_x). The small amount of F_y and F_z force would be mostly from blade entry/exit and buoyancy. Another finding to note is the nature of the centre of pressure; its location remains between the tip and the geometrical centre of the blade. The common assumption that it remains in the geometrical centre would drastically skew results if solely relying on bending strain gauges.

5.2 Recommendations

This system was proven to be a practical and functional analytical tool. It is recommended that it be fully utilized for stroke analysis with extended use by athletes and coaches. Its potential in this regard includes:

- assessment of ranging techniques and their efficiency
- adjustments of shaft length and bottom hand position and analyze torque and power effects
- matching athletes to their most effective blade size, shape, and style

These are relatively simple modifications and adjustments that athletes and coaches can make. The system provides the instantaneous feedback of how the adjustments affects efficiency, athlete power, or any other measurable parameter.

In addition to athlete and coaching, this system could assist for a biomechanical assessment of the athlete's stroke. Power produced by the athlete during a stroke could

be related back to the athlete's peak potential power in a lab setting. This would allow for an understanding of physiological efficiency which extends the possibility of improving performance. Ensuring that athletes train and utilized their force-velocity curve in an optimized manner is likely as significantly important as mechanical efficiency.

While a thorough display of parameter analysis was completed, it is difficult to provide any conclusive recommendations in terms of best stroke type. A more comprehensive set of stroke type data with a comparison of equipment, athletes, and test conditions is needed for a full stroke analysis. The purpose was to obtain a fully instrumented system and demonstrate its potential.

This system could be modified to better understand the hydrodynamics surrounding the blade, which would provide extra data to assist academic study and coaching. While it is not necessary for force decomposition, an accurate blade path profile is valuable and has yet to be measured. Video capture paths have been produced in the past [44, 50], however, their 2D post-process capture is tedious and not satisfactory in accuracy. This becomes clear with CFD results from video capture kinematics, where the highly sensitive nature of fluid modelling is greatly affected by moderate blade path error [43].

A number of methods are available to enable instantaneous blade path, such as ultrasonic sensors, infrared sensors, or multi-camera marker tracking. Extended Kalman filters have been recently used to achieve reasonably accurate position estimations with similar 9-DOF IMUs [66]. However, this method requires detailed filter modelling and is not a simple implementation task. If required, it is possible to improve an uncertainty by coupling devices which could provide a reliable and accurate blade path. In any event, blade position would provide an in-depth insight into the pull path and blade slip, which would allow more information on blade hydrodynamics.

Finally, a full assessment of blade mechanics would be to combine blade force and water flow measurements. Particle image velocimetry (PIV) is an obvious approach, but comes with numerous technical challenges. Particle seeding, illumination, and imaging are difficult tasks in a controlled lab setting let alone on-water.

Appendix A

Calibration

A.1 IMU

Improper IMU calibration can throw the orientation results to having an error so great that the data is unusable. The procedure to calibrate the IMU must look at each degree of freedom independently. The calibration collected samples of the three devices essentially finds the offset and scaled values of the measurement range. The procedure is as follows for each device using the Main IMU calibration.vi LabVIEW program:

A.1.1 The Accelerometer

The maximum and minimum readings of Earth's gravity each axis need to be found. These will be offset from the known value of 1 g and scaled with the accelerometer's set scale.

1. When ready, hold the indicated axis up (towards positive g) as close as possible. It may help to look at the data output to see where the axis maximum occurs.

2. Click the 'ready' button when the axis is pointing up. Very slowly move the device around to find the maximum reading for 5 seconds as indicated by the timer.

3. As displayed, do the same for the same axis but point it down (towards negative g).

4. Repeat 1-3 for each axis.
5. When finished click the Save button. Take the offset and scale results from the text file and enter it into the proper IMUcalibration.vi.

A.1.2 The Gyroscope

This is the easiest device to calibrate; all it needs to do is find the bias of rotation for each axis.

1. Select 'gyroscope'.
2. Place the IMU down and ensure it is motionless. This means checking if the table is vibrating, IMU wires are relaxed, etc.
3. Click the 'ready' button when ready and the program will begin collecting samples.
4. Unclick the 'ready' button after about 5 seconds to stop collecting samples.
5. Click the save button, the average of the samples will be displayed that will be saved for offset.

A.1.3 The Magnetometer

The magnetic profile of the surrounding area needs to be determined for a proper calibration of the magnetometer. Using Earth's magnetic field, maximum and minimum values need to be found of each axis and scaled -1 to 1. This means that any nearby electronic device or lights can affect the magnetometer reading. Therefore it is important to avoid putting any electronic devices near the IMU and calibrate in the environment that it will be used.

1. To start, select 'magnetometer'.
2. When ready, click 'collect samples'. The graph will then plot the x-y-z samples.
3. Motion the IMU around in random orientations to get 3 full circle profiles (x-y, x-z, y-z) as best as possible.
4. When done, unclick 'collect samples'. Remember to click 'calculate & save samples'.

A.2 Load Cell

The factory calibration for the load cell should already be completed, however, the bias needs to be set. This needs be done prior to any water trials and should be checked in-between every trial. To set or reset bias, hold the paddle vertically and ensure no load is acting on the paddle. Hit the 'zero' button on the load cell section of the Main.vi.

In addition, a pre-water trial and post-water trial check should be done to ensure load cell consistency. This is a three-point bending test; load the paddle with $\sim 20 - 30\,\text{lbs}$ where the bottom hand rests and support the paddle at the handle and blade by any rigid means. The key is to load the paddle using the exact same method before and after the testing trials. Compare results to ensure consistent readings.

Appendix B

Instrument Uncertainty

B.1 IMU

The LSM9DS0 IMU settings were:

- acceleration range $\pm 4\,\mathrm{g}$
- gyroscope rotation rate range $\pm 500\,^{\circ}/\mathrm{s}$
- magnetometer range $\pm 2\,\mathrm{gauss}$
- data rate $100\,\mathrm{Hz}$

The algorithm [4] fuses all the IMU data in real time into quaternion based orientation. A proportional and integral (PI) filter control is used and can be tuned to the device's need. The algorithm checks each reading and ensures orthogonality of the three devices and uses the PI filtering to fix drift. In this filter, gravity is used to orient itself to the up/down direction. When the device senses high acceleration, the accelerometer data is diminished or ignored because Earth's 1g orientation cannot be accurately determined.

In Figure B.1 the raw outputs of the IMU are shown. These correspond to the accelerometer (**a**), the gyroscope (**b**), and magnetometer (**c**). The data is from the same three strokes from the 1000 m test set as was shown in Figure 4.1 and 4.4. It is important to note that the data coming out of the accelerometer is quite noisy, the orientation algorithm described above successfully produces a smooth orientation output. Two tests were done in order to obtain an uncertainty of orientation; one static and one dynamic.

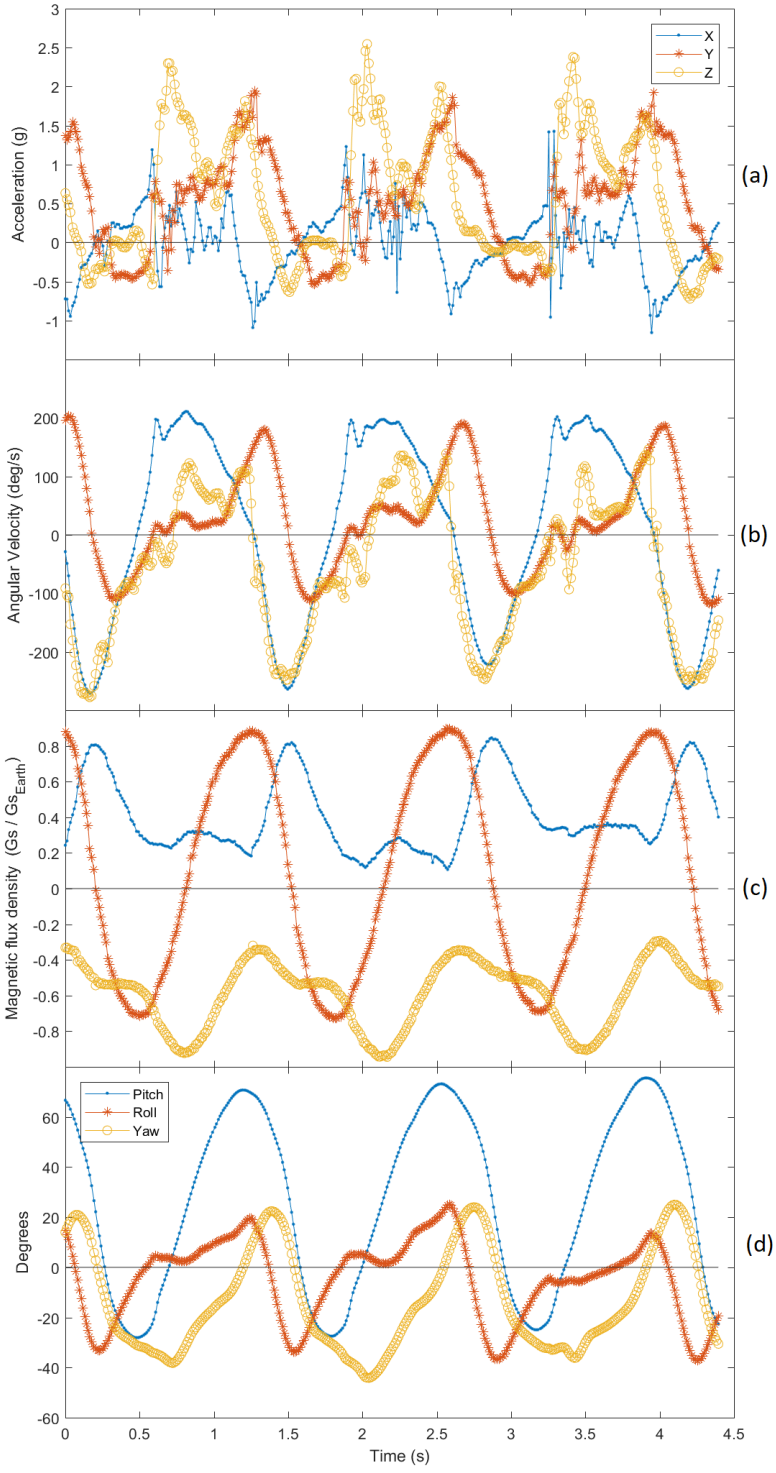

Figure B.1: The raw acceleration, gyroscope, and magnetometer data from the paddle IMU. Data sample is from the same three strokes as those in Figure 4.4, which is shown again here as **(d)**.

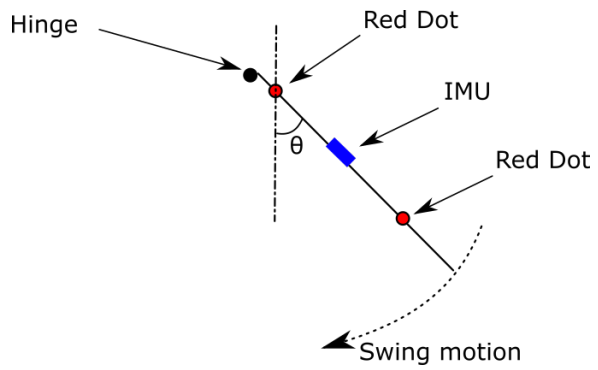

Figure B.2: The setup for the dynamic swing test to determine the IMU's accuracy of angle θ and to fine tune orientation algorithm parameters.

For the static test, an orientation grid sheet was drawn using a level and protractor tools. The IMU was then placed against the grid and the results were compared. It was found that the static results agreed with each other to well within 1° and did not drift.

A video swing test rig was constructed to determine the IMU's dynamic orientation accuracy. A hinge attached to a white swing rod, which was all mounted on a white background. The IMU was mounted on the swing rod along with two red indicator dots as shown in Figure B.2. A video camera roughly 3 m from the swing rig captured the swinging motion while IMU data transferred to the computer.

Post-processing of the video analyzed the angle that the red indicator dots created throughout the swing. The data was then compared to the IMU's pitch angle θ which can be seen in Figure B.3. It was found that an absolute maximum difference of 2.5° was present in the dynamic swinging, with a RMSD of ±1.5°. With this, it can be said that the IMU is capable of providing a reasonably accurate orientation angle of rotation rates similar to the paddle stroke.

B.2 GPS

A constant velocity accuracy is given by the GPS module manufacturer of 0.1 m/s, however changing velocity accuracy is unknown. This could be particularly problematic during rapidly changing velocities as seen in canoeing, which would deem the device as unreliable. An acceleration test was conducted using a bicycle in a clear area with an IMU attached to the spoke of the rear bike wheel. This provided a 'true speed' by

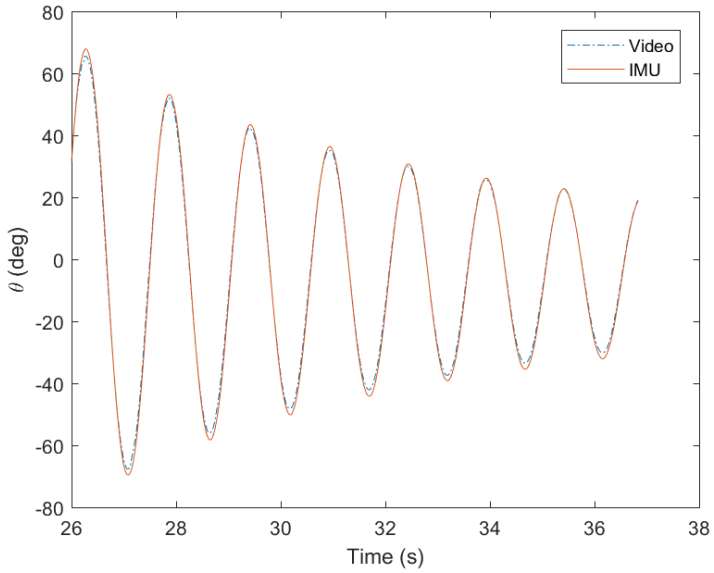

Figure B.3: The results of the dynamic IMU swing test, RMSD of true (video angle) and measured (IMU angle) is ±1.47°.

observing the minimum and maximum of two magnetometer axes which gave a wheel turn count. This was then compared with the GPS velocity which was fixed to the frame of the bicycle. The peak acceleration in this test was only 18% lower than the maximum acceleration observed during the real on-water tests.

It was found that the GPS matched the acceleration/deceleration of the bicycle well. The true speed vs GPS speed can be seen in Figure B.4. The two speeds had a maximum absolute error of 0.22 m/s or 6.7%. The RMSD of the sample is ±0.080 m/s. The manufacturer specified a lower accuracy of ±0.1 m/s, thus this quoted accuracy should be more appropriate.

B.3 Load Cell

To determine the accuracy of the force readings, the paddle is modelled as a simply supported beam, appropriately loaded, then results of expected and measured forces are compared. This was done by loading the paddle the paddle at the bottom hand location while the handle and blade were allowed to rest on sturdy stands to simulate the athlete's top hand and water force respectively. The amount of weight tested stepped up to 30 lbs, roughly 30% of force input by a top athlete. Excess static weight

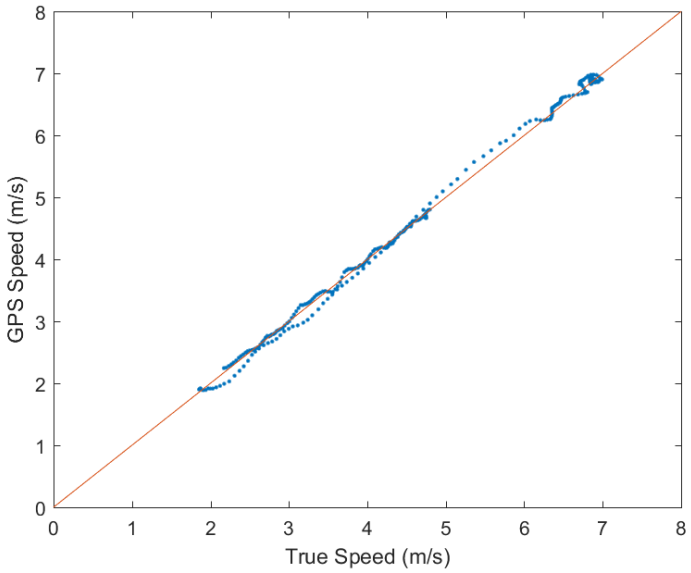

Figure B.4: The reading comparisons between true from the wheel and measured speed from the GPS, RMS of the error = 0.080 m/s, linear fit $r^2 = 0.998$.

could damage the paddle, thus a low value was used. Table B.1 shows the weights and resting positions used along with the expected and measured results. It is assumed that the other axes follow the same accuracy as the respective measured force and torque axis.

Another test looked at the distance between the load cell and the resting point on the blade and the predicted distance $d = T_y/F_x$, the results are shown in Table B.2. It appears that the error increases when the force is applied closer to the tip of the blade. Fortunately, this max error is still small (3%) and decreases as the force is applied

	F_x (N)			T_y (Nm)		
Load (lbs)	Expected	Measured	Err (%)	Expected	Measured	Err (%)
10	19.89	19.86	0.17	9.35	9.4	0.53
20	39.77	39.93	0.40	18.69	18.87	0.96
30	53.95	53.81	0.27	32.64	33.74	3.37
30	59.66	59.68	0.03	28.04	28.5	1.64
30	66.14	67.05	1.38	22.82	22.97	0.66

Table B.1: Simply supported beam loading test results. Force RMSD 0.42 N; torque RMSD 0.55 Nm.

Expected (cm)	Measured (cm)	Error (%)
34.5	34.19	0.89
46	45.89	0.22
47	47.46	0.99
51.5	52.62	2.19
60.8	62.67	3.08

Table B.2: Simply supported beam loading force (30 lbs) location results. Location RMSD: 1.0 cm

towards the centre of the blade. Therefore, it can be said that the load cell provides a sufficiently accurate prediction of the forces, torques, and applied locations.

B.4 Combined Device Uncertainty

Propulsive force F_P is an important measure in this thesis, and because it uses two measurement devices, its uncertainty should be evaluated. The transformation of F_x to F_P can be approximated as

$$F_P \approx F_x \cos\theta \tag{B.1}$$

The F_x and θ uncertainties evaluated previously. The uncertainty for F_P is found using propagation of errors [41], which is

$$\sigma_{F_P} = F_P \sqrt{\left(\frac{\sigma_{F_x}}{F_x}\right)^2 + \left(\frac{\sigma_{\cos\theta}}{\cos\theta}\right)^2} \tag{B.2}$$

At 0°, the θ uncertainty is negligible compared to σ_{F_x}. A problem arises since the $\cos\theta$ term is greatest when θ approaches 90°. At this high angle range, the angle uncertainty can be simplified as

$$|\cos(\theta \pm \sigma_\theta)| \approx \sin\sigma_\theta \approx \sigma_\theta$$

so the variation with θ is

$$\sigma_{\cos\theta} = \sigma_\theta |\sin\theta|$$

F_x (N)	θ (°)	σ_{F_P} (N)
75	-22	0.87
350	-14	2.3
230	50	4.6
110	63	2.6

Table B.3: A few selected data points throughout one sprint technique stroke to illustrate the maximum F_P uncertainty.

With this, Equation B.2 becomes

$$\sigma_{F_P} = F_P \sqrt{\left(\frac{\sigma_{F_x}}{F_x}\right)^2 + \left(\frac{\sigma_\theta \sin\theta}{\cos\theta}\right)^2}$$

Here, it becomes clear that when θ approaches 90° the error goes to infinity, however, F_P approaches zero at high angles. Therefore the error is bounded. A few sample points from the sprint technique are shown in Table B.3, showing that F_P remains within $\pm 5\,\text{N}$.

The power uncertainty σ_P can also be determined. From before,

$$P = F_B \omega L_B$$

where the ω uncertainty is determined as $2(\sigma_\theta)$. The power uncertainty is found by combining independent variables, where

$$\sigma_P = P \sqrt{\left(\frac{\sigma_{F_x}}{F_x}\right)^2 + \left(\frac{\sigma_\omega}{\omega}\right)^2 + \left(\frac{\sigma_{L_B}}{L_B}\right)^2} \tag{B.3}$$

An example using the sprint technique gives

$$P = (350\,\text{N})(4.6\,\text{rad/s})(1.68\,\text{m})$$

$$P = 2700\,\text{W}$$

Substituting this and the known uncertainties into Equation B.3, $\sigma_P = \pm 35\,\text{W}$.

Appendix C

Power & Blade Slip

From the review of literature, it appears that there is confusion of how blade slip affects hydrodynamics. The blade path through the water has been known for many years thanks to video capture. More recent numerical simulations have provided more insight on slip and its effect on power generation and efficiency. Before these simulations, a movement began in the early 1990s to use larger, wider blades. This was to reduce blade slip as it was believed to result in a loss of power [40, 12]. However, Nolte [46] countered that there must be blade movement through the water, otherwise no force can be put on the blade. Nolte also postulated through rowing video capture that blade slip at the start of the drive phrase would create a low pressure zone on the back face of the blade, creating a beneficial propulsive force through hydrodynamic lift. This seems to have been more recently proven to be somewhat true using CFD [55]. This means, the complex blade path and slip through the water can have a variety of effects, not all of which are negative, and could result in an overall gain of propulsive power.

Power is also often discussed in terms of propulsive power with respect to the stationary water, which is the dissipation of energy to the water [10]. This measures the force on the blade with its the velocity that it travels through the water. This inertial frame of reference, propulsive power, is the paddle dissipation and is defined as

$$P_{vs} = F_P v_s \tag{C.1}$$

where v_s is the propulsive blade slip velocity ($\omega L_B \cos\theta - V$), i.e. the velocity of the blade through the water. This can be seen in Figure C.1. Slip becomes negative during

late draw/early exit. At this phase, the blade is at a high pitch angle resulting in a high vertical component which gives a low propulsive component. The motion of the blade is therefore mostly vertical and a large negative slip velocity is seen. The negative slip translates to a negative blade slip power.

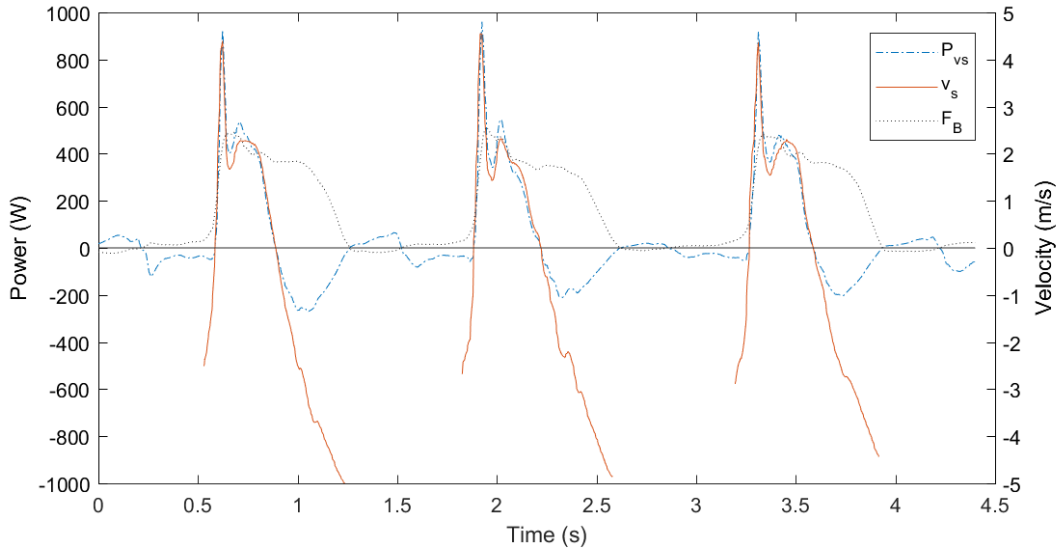

Figure C.1: Slip velocity v_s, or the velocity of the blade through the water, plotted with blade slip power P_{vs} during the 1000 m pace test. Blade force F_B is also shown as a scaleless reference.

At first glance, it appears that this can have big implications for performance; the late draw phase has negative propulsive work where the blade slip is negative. However, this blade slip should not expected to be accurate since blade velocity v_b is estimated as the angular pitch velocity from the top hand. The true slip velocity is a difficult measure, as it is difficult to define. The blade is slipping through the water at different rates throughout the blade face, thus any measure of this must come with a clear definition. Without proper blade path data, it is best to define power in terms of the athlete's reference frame.

Bibliography

[1] D. A. Aitken and R. J. Neal. An on-water analysis system for quantifying stroke force characteristics during kayak events. *International Journal of Sport Biomechanics*, 8(2):165–173, 1992.

[2] ATI Industrial Automation Inc. *Wireless Force/Torque Sensor System Installation and Operation Manual*, 9620-05-wireless ft-05 edition, Mar. 2015.

[3] J. Baker. Evaluation of biomechanic performance related factors with on-water tests. In *International Seminar on Kayak-canoe Coaching and Science*, pages 50–66, 1998.

[4] P. Bartz. 9 degree of measurement attitude and heading reference system, 2016. URL `https://github.com/Razor-AHRS/razor-9dof-ahrs`.

[5] A. Baudouin and D. Hawkins. A biomechanical review of factors affecting rowing performance. *British Journal of Sports Medicine*, 36(6):396–402, 2002.

[6] M. A. Berger. Determining propulsive force in front crawl swimming: a comparison of two methods. *Journal of Sports Sciences*, 17(2):97–105, 1999.

[7] S. Bifaretti, V. Bonaiuto, L. Federici, M. Gabrieli, and N. Lanotte. E-kayak: a wireless DAQ system for real time performance analysis. *Procedia Engineering*, 147:776–780, 2016.

[8] T. Buday. *Canoe technical template*. Canoe Kayak Canada, Sept. 2009.

[9] T. Bugalski. Hydromechanics for development of sprint canoes for the olympic games. In *Plastex: High Performances Print Boats and Paddles*. Ship Design and Research Centre S.A., 2010.

[10] D. Cabrera and A. Ruina. Propulsive efficiency of rowing oars. *Journal of Applied Biomechanics*, 2006. Submitted, unpublished.

[11] A. Campbell Ritchie and M. F. B. Selamat. Comparison of blade designs in paddle sports. *Sports Technology*, 3(2):141–149, 2010.

[12] N. Caplan. The influence of paddle orientation on boat velocity in canoeing. *International Journal of Sport Science and Engineering*, 3(3):131–139, 2009.

[13] N. Caplan and T. N. Gardner. A fluid dynamic investigation of the big blade and macon oar blade designs in rowing propulsion. *Journal of Sports Sciences*, 25(6):643–650, 2007.

[14] N. Caplan, A. Coppel, and T. Gardner. A review of propulsive mechanisms in rowing. *Proceedings of the Institution of Mechanical Engineers, Part P: Journal of Sports Engineering and Technology*, 224(1):1–8, 2010.

[15] L. W. Carr. Progress in analysis and prediction of dynamic stall. *Journal of Aircraft*, 25(1):6–17, 1988.

[16] A. Carter, J. Peach, T. Pelham, and L. Holt. Discrete measures of c-1 craft acceleration using various paddle designs. In *ISBS-Conference Proceedings Archive*, volume 1, 1994.

[17] F. Celentano, G. Cortili, P. Di Prampero, and P. Cerretelli. Mechanical aspects of rowing. *Journal of Applied Physiology*, 36(6):642–647, 1974.

[18] J. Coker. *Using a boat instrumentation system to measure and improve elite on-water sculling performance*. PhD thesis, Auckland University of Technology, 2010.

[19] M. Euston, P. Coote, R. Mahony, J. Kim, and T. Hamel. A complementary filter for attitude estimation of a fixed-wing UAV. In *Intelligent Robots and Systems, 2008. IROS 2008. IEEE/RSJ International Conference on*, pages 340–345. IEEE, 2008.

[20] N. Fleming, B. Donne, D. Fletcher, and N. Mahony. A biomechanical assessment of ergometer task specificity in elite flatwater kayakers. *Journal of Sports Science & Medicine*, 11(1):16, 2012.

[21] GlobalTop Technology Inc. *FGPMMOPA6H GPS Standalone Module Data Sheet*, v0a edition, 2011.

[22] B. Gomes, N. Viriato, R. Sanders, F. Conceição, J. P. Vilas-Boas, and M. Vaz. Analysis of the on-water paddling force profile of an elite kayaker. In *ISBS-Conference Proceedings Archive*, volume 1, 2011.

[23] W. Gutschow. Mechanik des getriebes ruderer/ruder. *Schiffstechnik*, 3:128–132, 1955.

[24] U. Hartmann, A. Mader, K. Wasser, and I. Klauer. Peak force, velocity, and power during five and ten maximal rowing ergometer strokes by world class female and male rowers. *International Journal of Sports Medicine*, 14(S 1):S42–S45, 1993.

[25] R. Helmer, A. Farouil, J. Baker, and I. Blanchonette. Instrumentation of a kayak paddle to investigate blade/water interactions. *Procedia Engineering*, 13:501–506, 2011.

[26] A. Hill. The heat of shortening and the dynamic constants of muscle. *Proceedings of the Royal Society of London Series B*, 126:136–195, 1938.

[27] S. R. Ho, R. Smith, and D. O'Meara. Biomechanical analysis of dragon boat paddling: A comparison of elite and sub-elite paddlers. *Journal of Sports Sciences*, 27(1):37–47, 2009.

[28] International Canoe Federation. Canoe sprint competition rules 2017, Jan. 2017.

[29] IOC. C-1 1000m (canoe single) men, 2016. URL `https://www.olympic.org/rio-2016/canoe-sprint/c-1-1000m-canoe-single-men`.

[30] IOC. C-1 200m (canoe single) men, 2016. URL `https://www.olympic.org/rio-2016/canoe-sprint/c-1-200m-canoe-single-men`.

[31] T. Ishiko. Biomechanics of rowing. In *Biomechanics II*, volume 6, pages 249–252. Karger Publishers, 1971.

[32] P. Jackson. Performance prediction for olympic kayaks. *Journal of Sports Sciences*, 13(3):239–245, 1995.

[33] R. Josephson. Contraction dynamics and power output of skeletal muscle. *Annual Review of Physiology*, 55(1):527–546, 1993.

[34] V. Kleshnev. Propulsive efficiency of rowing. In *ISBS-Conference Proceedings Archive*, volume 1, 1999.

[35] M. N. Macrossan. The direction of the water force on a rowing blade and its effect on efficiency. Technical report, The University of Queensland, 2008.

[36] M. N. Macrossan and N. W. Macrossan. Energy efficiency of the rowing oar from catch to square-off. Technical report, The University of Queensland, 2008.

[37] V. R. Mantha, A. J. Silva, D. A. Marinho, and A. I. Rouboa. Numerical simulation of two-phase flow around flatwater competition kayak design-evolution models. *Journal of Applied Biomechanics*, 29(3):270–278, 2013.

[38] T. P. Martin and J. S. Bernfield. Effect of stroke rate on velocity of a rowing shell. *Medicine and Science in Sports and Exercise*, 12(4):250–256, 1980.

[39] K. Mattes and N. Schaffert. New measuring and on water coaching device for rowing. *Journal of Human Sport and Exercise*, (II), 2010.

[40] J. S. Michael, R. Smith, and K. B. Rooney. Determinants of kayak paddling performance. *Sports Biomechanics*, 8(2):167–179, 2009.

[41] R. J. Moffat. Describing the uncertainties in experimental results. *Experimental Thermal and Fluid Science*, 1(1):3–17, 1988.

[42] A. F. Molland, S. R. Turnock, and D. A. Hudson. *Ship resistance and propulsion*. Cambridge University Press, 2011.

[43] D. Morgoch. Simulating the blade-water interactions of the sprint canoe stroke. Master's thesis, McMaster University, 2016.

[44] D. Morgoch and S. Tullis. Force analysis of a sprint canoe blade. *Proceedings of the Institution of Mechanical Engineers, Part P: Journal of Sports Engineering and Technology*, 225(4):253–258, 2011.

[45] D. Morgoch, C. Galipeau, and S. Tullis. Sprint canoe blade hydrodynamics-modeling and on-water measurement. *Procedia Engineering*, 147:299–304, 2016.

[46] V. Nolte. Introduction to the biomechanics of rowing. *FISA Coach*, 2(1):1–6, 1991.

[47] R. Pallard. Resistance experiments on sliding seat racing shells-part 1: Constant speed experiments. *St John's NL: NRC Institute for Marine Dynamics*, 1989.

[48] J. P. Peach, T. W. Pelham, A. G. Carter, L. Holt, and D. G. Burke. A method of motion analysis for self-propelled aquatic crafts. In *ISBS-Conference Proceedings Archive*, volume 1, 1995.

[49] T. Pelham, L. Holt, D. Burke, and A. Carter. Accelerometry for paddling and rowing. In *ISBS-Conference Proceedings Archive*, volume 1, 1993.

[50] S. Plagenhoef. Biomechanical analysis of olympic flatwater kayaking and canoeing. *Research Quarterly. American Alliance for Health, Physical Education, Recreation and Dance*, 50(3):443–459, 1979.

[51] M. G. Robinson, L. E. Holt, and T. W. Pelham. The technology of sprint racing canoe and kayak hull and paddle designs. *International Sports Journal*, 6(2):68, 2002.

[52] B. Sayer. *Rowing and sculling: The complete manual.* Edmundsbury Press Ltd, 1996.

[53] N. Schaffert, K. Mattes, and A. O. Effenberg. Listen to the boat motion: acoustic information for elite rowers. In *Human Interaction with Auditory Displays–Proceedings of the Interactive Sonification Workshop*, pages 31–38, 2010.

[54] S. Seiler. One hundred and fifty years of rowing faster. *Sportscience*, 10:10–45, 2006.

[55] A. Sliasas and S. Tullis. Numerical modelling of rowing blade hydrodynamics. *Sports Engineering*, 12(1):31, 2009.

[56] A. Sliasas and S. Tullis. A hydrodynamics-based model of a rowing stroke simulating effects of drag and lift on oar blade efficiency for various cant angles. *Procedia Engineering*, 2(2):2857–2862, 2010.

[57] A. Sliasas and S. Tullis. Modelling the effect of oar shaft bending during the rowing stroke. *Proceedings of the Institution of Mechanical Engineers, Part P: Journal of Sports Engineering and Technology*, 225(4):265–270, 2011.

[58] R. Smith and W. Spinks. Matching technology to coaching needs: On-water rowing analysis. In *ISBS-Conference Proceedings Archive*, volume 1, 1989.

[59] C. Soper and P. A. Hume. Towards an ideal rowing technique for performance. *Sports Medicine*, 34(12):825–848, 2004.

[60] R. C. Sprague IV, J. C. Martin, C. J. Davidson, and R. P. Farrar. Force-velocity and power-velocity relationships during maximal short-term rowing ergometry. *Medicine & Science in Sports & Exercise*, 39(2):358–364, 2007.

[61] E. Sprigings, P. McNair, G. Mawston, D. Sumner, and M. Boocock. A method for personalising the blade size for competitors in flatwater kayaking. *Sports Engineering*, 9(3):147–153, 2006.

[62] J. Stothart, F. Reardon, and J. Thoden. A system for the evaluation of on-water stroke force development during canoe and kayak events. In *4 International Symposium on Biomechanics in Sports (1986)*, 1986.

[63] D. Sturm, K. Yousaf, L.-Å. Brodin, and K. Halvorsen. Wireless kayak on-water ergometry–part 1: Paddle blade force. *Sports Technology*, 6(1):29–42, 2013.

[64] B. Tessendorf, F. Gravenhorst, B. Arnrich, and G. Tröster. An IMU-based sensor network to continuously monitor rowing technique on the water. In *Intelligent Sensors, Sensor Networks and Information Processing (ISSNIP), 2011 Seventh International Conference on*, pages 253–258. IEEE, 2011.

[65] J. Vos, H. Kimmich, J. Mäkinen, H. Ijsenbrandt, and J. Vrijens. Telemetry of dynamic forces in endurance sports. In *Biotelemetry II*, pages 106–108. Karger Publishers, 1974.

[66] G. Zizzo and L. Ren. Position tracking during human walking using an integrated wearable sensing system. *Sensors*, 17(12):2866, 2017.